BIODIVERSITAS
Volume 26, Number 9, September 2025
Pages: 4577-4597

ISSN: 1412-033X
E-ISSN: 2085-4722
DOI: 10.13057/biodiv/d260929

Biomass mapping for wildlife management using UAV-satellite integration and deep learning in Kui Buri National Park, Thailand

JEDSADA NOOWONG[1], WARONG SUKSAVATE[1], VISANUWIT THONG-ON[2], NOPPORN AKKAMANEE[3], ATTAPONG PAO-ON[3], KORNSORN SRIKULNATH[1,4], PRATEEP DUENGKAE[1,4,♥]

[1]Special Research Unit for Wildlife Genomics (SRUWG), Department of Forest Biology, Faculty of Forestry, Kasetsart University. 50 Phahonyothin Rd., Chatuchak District, Bangkok 10900, Thailand. Tel.: +66-2-579-0176, Fax.: +66-2-942-8107, ♥email: fforptd@ku.ac.th
[2]World Wide Fund for Nature International-Thailand (WWF-Thailand). Pradiphat Rd., Phayathai District, Bangkok 10400, Thailand
[3]Department of National Parks, Wildlife and Plants Conservation. 61 Phaholyothin Rd., Chatuchak District, Bangkok 10900, Thailand
[4]Animal Genomics and Bioresource Research Unit (AGB Research Unit), Faculty of Science, Kasetsart University. 50 Phahonyothin Rd., Chatuchak District, Bangkok 10900, Thailand

Manuscript received: 12 June 2025. Revision accepted: 22 September 2025.

Abstract. *Noowong J, Suksavate W, Thong-On V, Akkamanee N, Pao-On A, Srikulnath K, Duengkae P. 2025. Biomass mapping for wildlife management using UAV-satellite integration and deep learning in Kui Buri National Park, Thailand. Biodiversitas 26: 4577-4597.* In recent years, remote sensing has become a widely adopted tool for grassland management, offering advantages in assessing spatiotemporal dynamics. However, sample collection within satellite grids presents limitations because ground samples may not fully represent the corresponding satellite pixels. To address this challenge, the present study aimed to reduce sampling error by bridging ground-scale observations with satellite-scale data using digital images, Unmanned Aerial Vehicle (UAV) imagery, and Sentinel-2 for grass biomass estimation. A Convolutional Neural Network (CNN) was used to classify biomass from digital images and UAV imagery, whereas a random forest algorithm was utilized to link these classifications to freely available Sentinel-2 imagery. The study was conducted in cultivated grasslands managed for mitigating human-wildlife conflict in Kui Buri National Park, Thailand. The results showed that a pre-trained CNN model based on digital images (MAE±0.351 classes) successfully transferred to UAV imagery using fine-tuning. When scaled to the satellite level, the model explained 94% of the variance (R^2), with RMSE = 8.56 g/m^2. The grassland yield was lowest during the dry season, with a minimum value in March of 34.82±0.09 g/m² (67.12±0.33 tons/month), while it reached a peak during the wet season in November at 110.03±0.32 g/m² (212.06±1.19 tons/month). These finding demonstrate the ecology of ruzi grass under natural conditions with free-ranging wildlife grazing. Overall, the study highlights a viable strategy for bridging ground and satellite scales to reduce sampling error and proposes a novel approach to monitoring grassland yield at very high spatial resolution and high precision, while providing evidence of overgrazing and gaur overpopulation in the grasslands. Grazing rotation management was suggested to restore degraded grassland, and enhance the potential yields of the grassland. By integrating ecological insights with practical management recommendation, this study contributes to sustainable grassland restoration and wildlife conservation strategies.

Keywords: Biomass estimation, convolutional neural network, digital image, remote sensing, UAV imagery

INTRODUCTION

Remote Sensing (RS) technology has been widely utilized to evaluate biomass, offering broad spatial coverage, repeatability, cost-effectiveness, and the ability to assess temporal dynamics across scales (Boyd and Danson 2005; Kumar and Mutanga 2017; Dong et al. 2020). Importantly, direct measurement of Above Ground Biomass (AGB) across freely available satellite imagery lacks the spatial resolution needed to capture fine-scale ground features (e.g., 15 × 15 m for Sentinel-2), and sampled areas may not fully represent the satellite pixels. Sampling errors also arise when plot sizes are smaller than the satellite grid, especially in areas with substantial local spatial variability in plant life forms such as the naturally heterogeneous environments examined in this study site (Baccini et al. 2007; Réjou-Méchain et al. 2014; Araza et al. 2022).

To address these limitations, we utilized Unmanned Aerial Vehicle (UAV) imagery provided very high-resolution information on ground features (Zhu et al. 2024). UAV-based multispectral imagery provides Vegetation Indices (VIs) that are strongly correlated with AGB (Schirrmann et al. 2016a; Amorim et al. 2022). However, UAV deployment is costly due to sensor and software expenses, battery limitations restrict coverage of large areas, and assessing temporal dynamics further increases costs.

To overcome these constraints, digital images were used to estimate AGB at the ground scale, offering a low-cost and flexible alternative (Ma et al. 2019). Satellite imagery was then utilized to upscale the analysis, leveraging its broad coverage and temporal resolution. To bridge the gap between ground scale to the satellite scale, low-cost UAVs equipped with RGB sensors were used to link digital images with satellite data by capturing imagery in only some areas throughout all seasons, thereby reducing costs (Schirrmann et al. 2016b).

Kui Buri National Park (969 km^2), located within the Kaeng Krachan Forest Complex, was designated a UNESCO Natural World Heritage site in 2021 (UNESCO 2021). It supports one of the largest remaining populations of Asian elephants (*Elephas maximus* (Linnaeus, 1758)) in the Tenasserim Range (Parr et al. 2008). Human-wildlife

conflict (elephants and gaurs) is common in the surrounding buffer zone (Parr et al. 2008; Tanasarnpaiboon 2016). After the killing of four elephants by farmers in 1997, the "Conservation and Restoration of Kui Buri Forest Project" was launched in 1998 as part of Thailand's Royal Project system. The project focused on reducing crop raiding by restoring degraded land and establishing forage-rich grasslands to support elephant populations within protected boundaries. The project assumes that crop raiding is linked to fodder availability in forests and croplands (Srikrachang and Srikosamatara 2005). As a solution, approximately 16 km^2 of cropland were allocated to the national reserved forest to improve elephant habitat through the cultivation of nutritious forage grasslands (1.93 km^2), pond construction, and reforestation of degraded areas. Currently, ruzi grass (*Brachiaria ruziziensis* R.Germ. & C.M.Evrard), an alien species introduced by national park staff, is the dominant species. The park now serves as a national model for collaborative wildlife tourism and habitat management (Phumsathan and Pongpattananurak 2021).

Rangelands are ecosystems dominated by grasses, forbs, and shrubs that provide essential energy and nutrition for herbivores, making them a central focus of habitat management (Holechek et al. 2010; Bleich et al. 2020; Cinar et al. 2020). Forage biomass is a key indicator of habitat quality and a manageable environmental factor for habitat improvement. High forage biomass promotes habitat use and reproduction by ungulates (Paansri et al. 2022). However, the grassland yield in Kui Buri National Park has not yet been evaluated.

The present study examines the seasonal dynamics of forage biomass in cultivated grassland. It demonstrates that digital images and standard UAVs are sufficient for estimating AGB with high precision. Biomass data from temporal plots were analyzed using a Convolutional Neural Network (CNN) applied to RGB digital and UAV imagery, then linked to Sentinel-2 satellite data via Random Forest (RF) modeling. The findings offer new strategies for high-precision biomass estimation under natural conditions for similar studies elsewhere and guiding habitat management priorities. Moreover, the results provide ruzi grass ecology under natural conditions and contribute to more effective grassland management through near-real-time monitoring data that requires only cloud-free Sentinel-2 data. These new strategies are critical for mitigating human-wildlife conflict caused by large herbivores leaving protected areas.

MATERIALS AND METHODS

Study area

This research was conducted on cultivated grasslands managed for wildlife within the national forest reserve adjacent to the eastern-central boundary of Kui Buri National Park (Prachuap Khiri Khan Province, Thailand), under the supervision of park authorities. The grassland was divided into two management zones: a wildlife tourism zone (covering the majority of the area; 1.33 km^2) and a no-wildlife tourism zone (0.60 km^2). The grassland is located at 12°10′33″N, 99°38′56″E and covers approximately 1.93 km^2, which was chosen as the boundary for biomass mapping. A buffer zone extending 200 m from the grassland was included to study the distribution of ruzi grass outside cultivated zone, totaling approximately 6.68 km^2 (Figure 1). The predominant habitats are dry evergreen forest, mixed deciduous forest, and tropical rainforest (Kui Buri National Park 2003; Temchai et al. 2010).

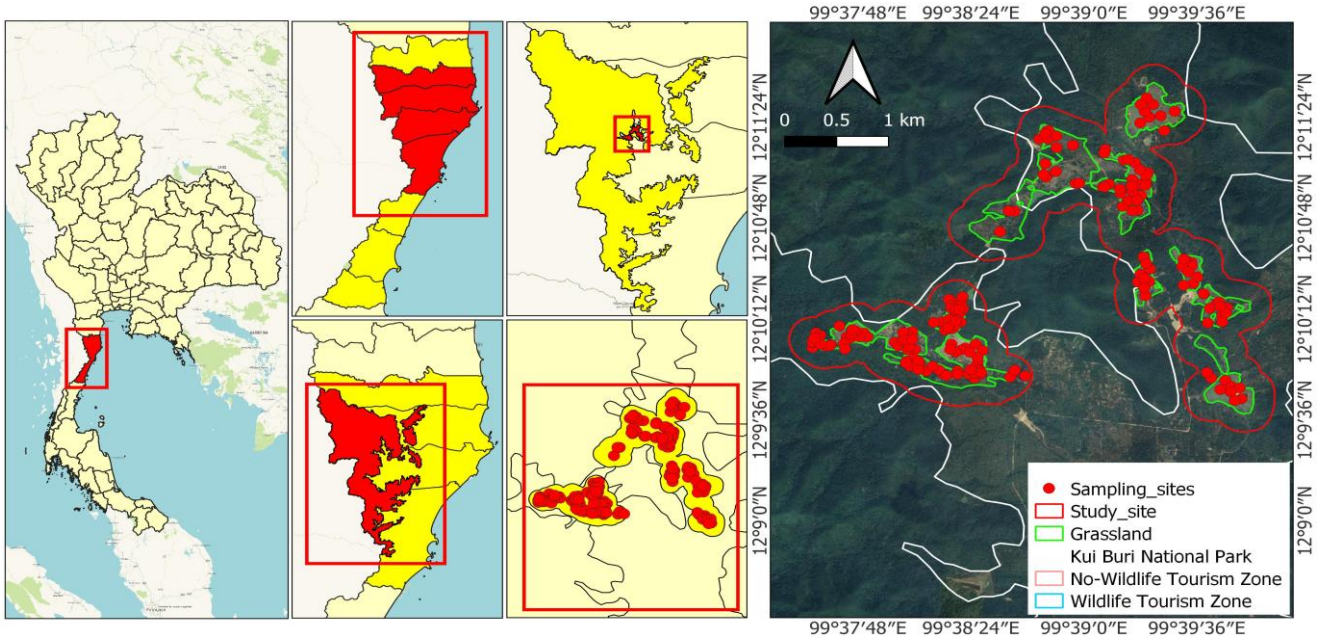

Figure 1. The study site in the grassland of Kui Buri National Park, Thailand. The majority of the grassland is managed as a wildlife tourism zone (upper part), while the lower part is designated as a non-tourism zone

Seasonal classification followed a modified scheme from Tanasarnpaiboon (2016), based on precipitation and temperature data from the Thai Meteorological Department (2014): May to December was defined as the wet season; January to April was defined as the dry season. Elevation within the grassland ranges from 127 to 301 m, with an average of 174 m. The province receives approximately 918 mm of annual precipitation, with temperatures ranging from 18°C to 37°C (Thai Meteorological Department 2014; Tanasarnpaiboon 2016).

Sampling site classification

Sampling sites were categorized into 20 land cover types using K-means clustering based on Sentinel-2 imagery from 2021-2022, capturing annual grassland dynamics prior to fieldwork. The number of land cover types was chosen based on the ability of collecting 13-15 sampling sites per month. While aiming to collect 2 spatial replicates per land cover types. Among the 20 land cover types, seven land cover types represent the annual forage dynamics within the grassland. The most recent satellite imagery, acquired within 5 days of field sampling, was grouped with these land cover types using Euclidean distance. Sentinel-2 imagery were exported from Google Earth Engine (GEE) at a resolution of 15 × 15 m per grid cell, matching the sampling plot size (Paansri et al. 2021) (Figure 1). All analyses were conducted in RStudio (R Core Team 2018). Land cover types were distinguished by gradient of vegetation cover. Land cover types 5, 7, 11, 13, 14, 16, and 18 represent the annual forage dynamics within the grassland and the composition of forage types, while the remaining land cover types correspond to other features such as forests, building and water bodies.

Field data acquisition

Figure 2 presents the overall workflow of the grass biomass estimation model. The first step involves field data collection, including biomass measurement and the capture of digital and UAV images. Second, biomass values are classified based on digital images using a CNN model and transferred to UAV imagery. Finally, the ground-scale model is bridged to the satellite scale via a RF model, using UAV-based biomass as samples.

Field data was collected during September 2023 to October 2024 followed a model-based sampling strategy. At each sampling site, four 1 × 1 m temporal plots were established 5 m from the site center. Each plot was subdivided into four 50 × 50 cm subplots, yielding 16 subplots per site (Figure 3). Between 13-15 sampling sites were measured each month, without repeated measurements at previously sampled sites. All forage crops within subplots were clipped and sorted into four categories: ruzi grass, other grass species, forbs, and shrubs (Holechek 1984). Fresh biomass was oven-dried at 70°C for 48 h to determine dry biomass (Vawda et al. 2024). For each subplot, the height of six ruzi grass height was measured, including three visibly grazed and three ungrazed samples, to assess the impact of herbivory on forage structure. In total, 188 temporal sampling sites, 752 plots, and 3,008 subplots were established; however, 4 subplots could not be captured with digital camera due to rainy conditions.

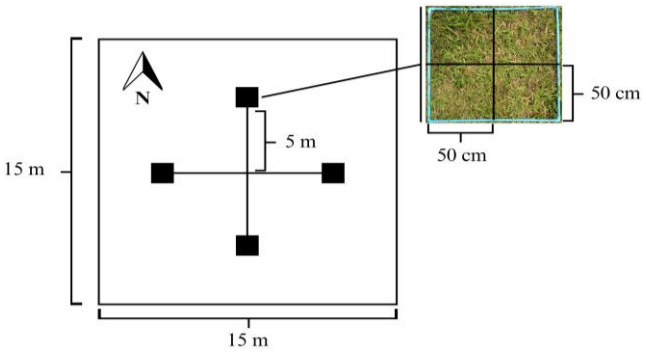

Figure 3. Four 1 × 1 m plots were established 5 m from the site center at each sampling site and were subdivided into sixteen 50 × 50 cm subplots

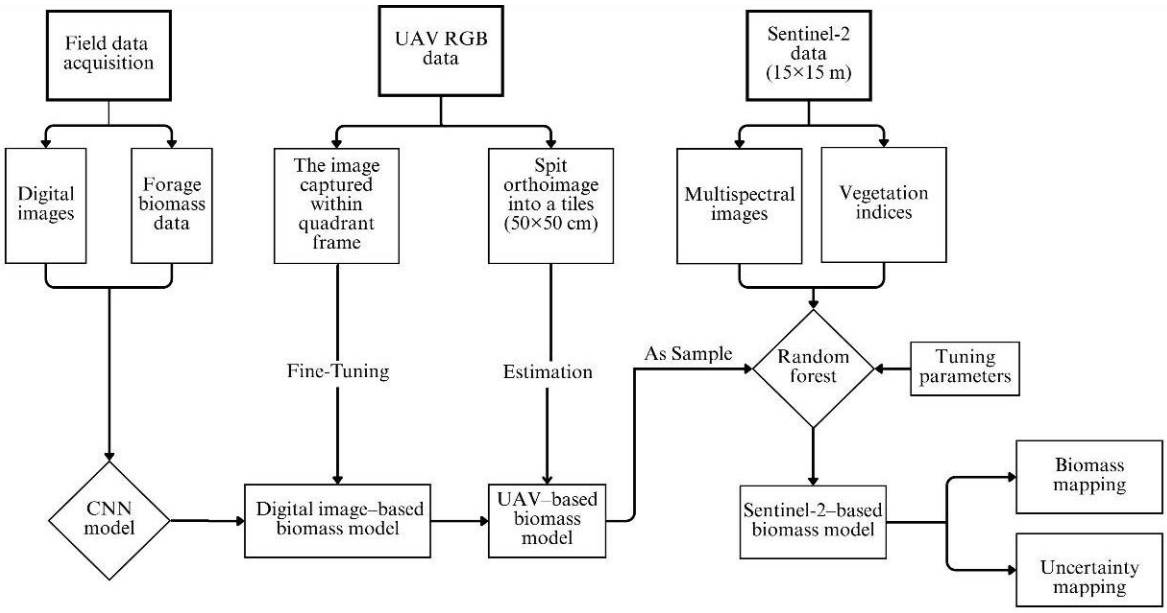

Figure 2. Overall workflow of the grass biomass estimation model (process steps shown from left to right)

Digital and UAV image acquisition and processing

Digital images were captured using Nikon D7500 and Nikon D7000 cameras. For each subplot, images (digital images and UAV imagery) were taken before clipped with the camera positioned parallel to the ground (Figure 5). Each image was manually cropped to fit the 50 × 50 cm quadrant frame, resulting in dimensions of approximately 2,300 × 2,300 pixels (0.217 mm/pixel), and saved in JPEG format.

The UAV survey flights, including field data acquisition, were conducted with authorization from the Department of National Parks, Wildlife and Plant Conservation, and were operated by a certified UAV pilot. UAV imagery was acquired during March 2024 to October 2024 using a DJI Mavic 3 Enterprise Thermal at varying flight altitudes (25-60 m). Each raw UAV scene image resolution was 4,000 × 3,000 pixels. Photogrammetric processing was performed using DJI Terra software (DJI, Shenzhen, Guangdong, China; DJI 2025).

The dry biomass of grass (ruzi grass, and other grass species) was the primary target output, whereas that of forbs and shrubs was considered auxiliary data. Forbs and shrubs were rarely grazed at the site, and ungulates strongly avoided shrubs due to the lack of mechanisms to mitigate their toxicity (Cappai and Aboling 2020). Grass biomass values exceeding 0.4 (>101.2 g/m^2, normalized without outliers) could not be reliably estimated and were capped at 0.4 in the regression model. Thus, classification was deemed more appropriate than regression. Biomass values were grouped into three ordinal classes using K-means clustering for ground-scale model. Due to the decision to use a small image size (22 × 22 pixels), the available feature data were insufficient to accurately classify a narrow range of biomass classes (more than three classes). Based on trial and error testing with images 22 × 22 pixels using RGB bands, found that three biomass classes predictions provided the most optimal result. Biomass values below 0.4 were split into two classes, and values above 0.4 formed a third class. Class sizes were balanced by digital image count (Table 1 and Figure 4).

Convolution neural network

Although there are various algorithms for classification tasks, such as RF (Breiman 2001), logistic regression (Cox 1958), Support Vector Machines (SVM) (Boser et al. 1992; Vapnik 1995), and Artificial Neural Networks (ANN) (Dong and Hu 1997), deep neural networks consistently outperform these methods in image recognition (Beohar and Rasool 2021). CNNs constitute an advanced form of ANN designed to extract complex visual features such as shape, structure, and color to the deciphering of intricate patterns and relationships from input data (Zhu et al. 2017; Marcus 2018; Kattenborn et al. 2021); they are widely used in remote sensing for biophysical estimation and land cover classification (Mas and Flores 2008; Jensen et al. 2009).

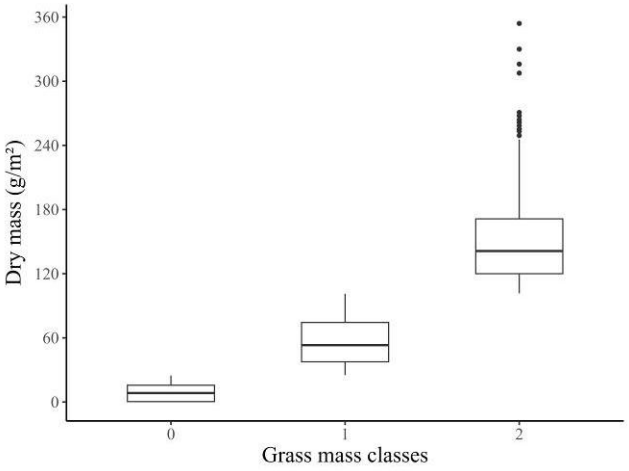

Figure 4. Boxplots showing the distribution of dry target biomass values for each biomass class. The black dots represent dry mass data points beyond the upper inner fence (third quartile + 1.5 × interquartile range), referred to as outliers

Figure 5. The image samples were captured at subplots measuring 50 × 50 cm, with the camera positioned as parallel to the ground as possible to ensure a consistent perspective

Table 1. Descriptive statistics of dry target biomass each classes output (g/m^2) for ground-scale model (digital image)

Classes grass	Number of images	Mean	Median	SD.	SE.	Max	Min
0	1,082	9.08	8.40	7.91	0.24	24.80	0
1	1,094	57.10	53.20	22.37	0.67	101.20	25.20
2	828	150.30	141.20	37.94	1.31	354.00	101.60

Compared to conventional machine learning models, CNNs are more suitable for biomass estimation in heterogeneous forage environments (Schreiber et al. 2022). CNNs automatically extract features such as shape, structure, and color and have an enhanced capability to process images in their original form (two-dimensional or three-dimensional structured data). In contrast, conventional machine learning suffers from the selectivity-invariance problem, requires manual feature engineering for image feature extraction, and incurs high computational costs in runtime and/or memory (Nargesian et al. 2017; Chauhan and Singh 2018). While conventional machine learning models have an advantage in interpretability, CNNs are more difficult to interpret. However, this study does not aim to determine the relative importance or contribution of each feature (e.g., RGB values) to the classification (Chehade et al. 2022). Therefore, CNNs were chosen for this study.

Input images were resized to 22 × 22 pixels with RGB bands (2.27 cm/pixel), corresponding to the minimum pixel size of UAV imagery for 50 × 50 cm subplots. This resizing involved a trade-off between obtaining the highest possible number of UAV imagery samples for subplots (452 images) and significantly losing image features. The maximum resolution of UAV imagery for subplots is 50 × 50 pixels, but this resolution yielded very few samples (approximately 70 images). However, preliminary experiments with larger image sizes showed no significant improvement in performance compared to using 22 × 22 pixels input images (Table 5).

Because dry biomass values were grouped into ordinal classes, the Conditional Ordinal Regression for Neural networks (CORN) method was selected for loss calculation and grade prediction, using a chain rule of probabilities (Shi et al. 2023). The model architecture, iteratively developed through trial and error, is illustrated in Figure 6. The ordinal output layer was implemented using the CornOrdinal and CornOrdinalCrossEntropy functions from the coral_ordinal package in TensorFlow (Shi et al. 2023). Ordinal labels (q) were predicted using cumulative binary task probabilities:

$$q = 1 + \sum_{k=1}^{K-1} 1\{f_k(X^i) > 0.5\}.$$

Where :

$f_k(X^i) \in [0,1]$: Predicted probability of the $k-th$ binary classification subtask

$1\{.\}$: Returns 1 if $f_k(X^i) > 0.5$, otherwise, it returns 0

To fine-tune the model on a small training dataset, image augmentation was conducted (Shorten and Khoshgoftaar 2019). This technique enhances dataset diversity, increases the effective training size, improves model performance, and reduces the risk of overfitting (Krizhevsky et al. 2017; Poojary et al. 2021). Augmentation was performed using the ImageDataGenerator function from the TensorFlow package, with parameters listed in Table S1. Additional custom parameters included random noise, random shuffling of quadrant images, and random shadow effects. Parameter ranges were selected to ensure that both original and augmented images remained visually recognizable. Augmented images were designed to simulate varied scenarios and conditions that could realistically occur during field data collection (Decitre and Joyce 2024). Hyperparameters were selected via trial and error under limited computational resources. The initial learning rate was set to 0.0005 and reduced every five epochs by a factor of 0.75, with a minimum threshold of 0.000001. A mini-batch size of 16 was used. The model was trained for 50 epochs using the Adaptive Moment Estimation (Adam) optimizer to update network weights (Kingma and Ba 2014). The dataset for digital image was split into training, validation, and test sets at a ratio of 80:10:10.

Model performance was evaluated using the Mean Absolute Error (MAE) and a confusion matrix. The equation for MAE is as follows:

$$\mathrm{MAE} = \frac{1}{N}\sum_{i=1}^{N} |y_i - h(x_i)|$$

Where :

y_i : True label of the i-th sample in the test dataset

$h(x_i)$: Predicted label

N : Total number of samples in the test dataset (Shi et al. 2023)

The best-performing model was selected based on the lowest MAE observed in the validation dataset. The CORN model was implemented using the coral_ordinal package in Python 3.8 and TensorFlow 2.8.4; it was trained on a workstation equipped with an NVIDIA GeForce RTX 4070 SUPER GPU and 64 GB RAM.

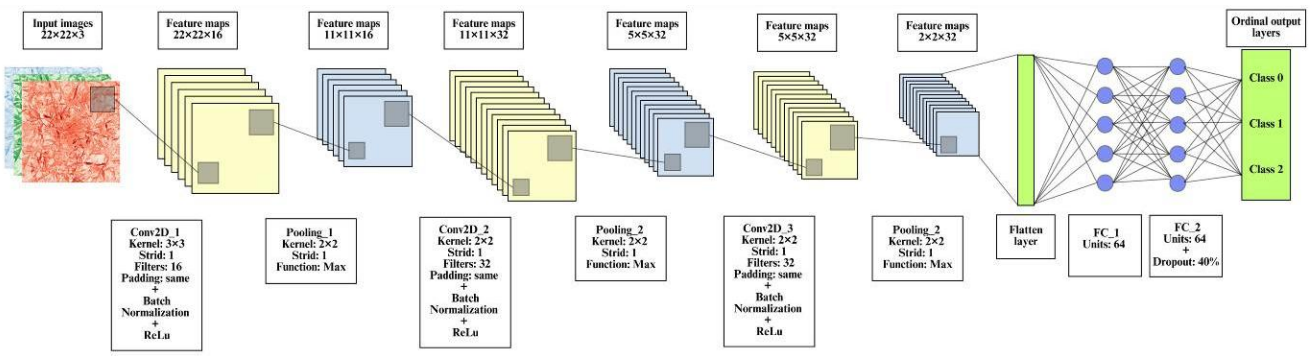

Figure 6. The architecture of the CNN model is based on digital imagery (RGB features) as input for classifying grass biomass classes

Transfer of learning to UAV imagery

The digital image-based CNN model was transfer to UAV imagery because UAV provide broader spatial coverage. Direct transfer of the digital image-based CNN model to UAV imagery was not feasible due to differences in source domain characteristics, including lighting conditions, brightness, object scale, and resolution (Gao et al. 2024). To address this transfer barrier, a fine-tuning technique was utilized based on the pre-trained digital image CNN model (Shin et al. 2016). In total, 451 UAV images (0.94-2.27 cm/pixel), each captured using a 1 × 1 m quadrant frame, were cropped to 50 × 50 cm and resized to 22 × 22 pixels (2.27 cm/pixel). These images were split into training, validation, and test datasets at a 70:10:20 ratio. The test dataset was entirely unseen during training for both the digital image and UAV-based models. The learning rate was initially set to 0.00005 and reduced every five epochs by a factor of 0.75. A mini-batch size of 8 was used; the fine-tuned model was trained for 30 epochs using the Adam optimizer. Image augmentation was conducted to improve generalization. For prediction, UAV map areas (15 × 15 m) without tree cover or water bodies were selected. These maps were divided into 50 × 50 cm tiles (22 × 22 pixels) and classified using the fine-tuned CNN model, which had been pre-trained on digital images captured from ground-level subplots.

Satellite-based biomass mapping using Sentinel-2 imagery

The biomass map derived from UAV imagery was upscaled to 15 × 15 m resolution across the study area by summing the median biomass class values within each Sentinel-2 grid cell without tree cover or water bodies, which served as the sample dataset for satellite-based modeling (Mao et al. 2022; Ge et al. 2024; Niu et al. 2024; Zhu et al. 2024) (Figure 2). A spatial resolution of 15 × 15 m was selected for Sentinel-2 data match the sampling site size, rather than the official 10 × 10 m resolution. Moreover, not all bands have a 10 × 10 m spatial resolution, as the reflectance bands vary in spatial resolutions (i.e., 10 × 10 m, 20 × 20 m, and 60 × 60 m) (CDSE 2017). VIs were selected based on prior studies demonstrating strong correlations with grass biomass (Kobayashi et al. 2020; Vawda et al. 2024). Median values of Sentinel-2 reflectance bands and VIs were exported and calculated from GEE, using imagery acquired as close as possible to field observation dates under cloud-free conditions. The selected indices are listed in Table S2.

An RF model (Breiman 2001) was developed to establish the relationship between Sentinel-2 imagery (including VIs) and grass biomass (Singh et al. 2015). Two key parameters—namely, the number of bootstrap decision trees (ntree) and the number of variables used to split each node (mtry)—were tuned to optimize model performance (Wang et al. 2016). The ntree parameter was varied from 500 to 3,000 in increments of 100; mtry was varied from 6 to 14 in increments of 1. Model tuning was performed using the H2O package in RStudio (Aiello et al. 2016; R Core Team 2018).

The UAV-derived dataset was stratified by month of acquisition and split into training, validation, and test datasets at a 80:10:10 ratio. The optimal RF model was selected based on the lowest Root Mean Squared Error (RMSE) observed in the validation set. Model performance was evaluated using the coefficient of determination (R^2) from linear regression, RMSE, and normalized RMSE (NRMSE) (Rischbeck et al. 2016). The equations for RMSE and NRMSE are as follows:

$$\mathrm{RMSE} = \sqrt{\frac{1}{N}\sum_{i=1}^{N}(|y_i - y|)^2}$$

$$\mathrm{NRMSE} = 100 \times \frac{\sqrt{\frac{1}{N}\sum_{i=1}^{N}(|y_i - y|)^2}}{\bar{y}}$$

Where :

y_i : Observed value

y : Predicted value

$\bar{y}$: Mean observed value

N : Number of observed values

The grass biomass distribution maps were predicted for open areas lacking tree cover or water bodies within grid cells (the remaining 3,335 grids from a total of 8,566 of the grassland, covering about 0.75 km^2) using monthly multispectral data and VIs from Sentinel-2 imagery under cloud-free conditions throughout the year 2024 and based on median values. The uncertainty maps were produced to evaluate the quality of the biomass map generated from the optimal RF model. These maps were created by calculating the Coefficient of Variation (CV) for each pixel, based on the predictions from all independent trees in the optimal RF model (700 trees in optimal RF). A high CV value indicates high uncertainty, meaning that the independent trees are not in agreement—some predicted low values while others predicted high values (Huechacona-Ruiz et al. 2020). The uncertainty maps and grass biomass distribution maps were performed using the randomForest package in RStudio (Liaw and Wiener 2002).

The modeling process was conducted in RStudio using the terra (Hijmans 2025), rsample (Frick et al. 2025), and tidyverse (Wickham et al. 2019) packages. Statistical plots were generated using the ggplot2 package in RStudio (Wickham 2016). Map visualization was performed using QGIS software version 3.30 (QGIS.org 2025).

Estimation of grassland carrying capacity

The CC of grassland was assessed based on grass biomass yield to determine the potential of the area to sustainably support animal populations (De Leeuw et al. 2019). It was calculated using the equation proposed by Holechek et al. (2010):

$$\mathrm{CC} = \frac{\mathrm{AGB}}{S_f \times G_t}$$

Where :

AGB: Grassland yield (kg)

S_f : Daily dry mass intake per individual per day (kg per day)

G_t : Grazing time, defined as 30 days (calculated per month)

The Relative Stocking Density (RSD) was calculated via division of animal units by CC (Piipponen et al. 2022).

The RSD was classified into four levels to determine grassland CC status. Values of <0.8, 0.8-1.0, 1.0-1.2, and >1.2 were defined as "unexploited," "normal," "overexploited," and "seriously overexploited," respectively (Dong et al. 2019).

Due to continuous grazing, ruzi grass in the grassland remained short throughout the year; the highest average height was observed in November at 11.9±0.16 cm (SE), whereas the shortest was observed in April at 5.28±0.08 cm. Such low height negatively affects grass availability and intake for elephants. Baskaran et al. (2010) reported that when grass height is too low (<10 cm) for the trunk to grasp, elephants resort to scraping the grass using their forefoot toenails. This behavior indicates that elephants utilize ruzi grassland to a much lesser extent compared with gaur. Additionally, short grasses are generally consumed when their height is around 50 cm (Sukumar 1990). Wild Asian elephants prefer browsing over grazing, and bamboo is a major component of their diet when abundant, as observed in Kui Buri National Park (Chen et al. 2006; Himmelsbach et al. 2006; Joshi and Singh 2008; Temchai et al. 2010; Schwarz et al. 2020). Consequently, the CC was assessed exclusively for gaur because ruzi grassland provides limited forage availability for elephants.

Monthly grassland yield was calculated based on the 95% confidence interval of Sentinel-2-based grass biomass and converted to the entire grassland area (1.93 km^2). For daily intake data of gaur, body weight was used to estimate minimum dietary requirements. Stuth and Sheffield (1986) reported that herbivores with a body weight ranging from 500 to 1,000 kg require daily dry matter intake equivalent to 3% of their live weight. The weight of adult bulls was reported to range from 600 to 1,000 kg (average 800 kg) (Ashokkumar et al. 2011). Consequently, dry mass dietary intake was estimated to be approximately 24 kg/day.

RESULTS AND DISCUSSION

Descriptive statistics of forage biomass

Observed dry forage biomass was measured at 188 sampling sites from September 2023 to October 2024. Table 2 and Figure 7 presents forage ecology by month. Ruzi grass was the predominant life form in the grasslands, followed by forbs, other grass species, and shrubs, respectively. The biomass of ruzi grass was high during the wet season (May-December) and decreased significantly during the dry season (January-April). During the wet season, ruzi grass exhibited high dry biomass, averaging 73.93±1.44 g/m^2, with a peak value of 354 g/m^2 in October. In contrast, productivity during the dry season was low, averaging 16.26±0.62 g/m^2; the lowest biomass was recorded in April at 0.4 g/m^2. The seasonal trends of forbs, other grass species, and shrubs mirrored those of ruzi grass.

Table 2. Descriptive statistics of observed seasonal forage biomass by season (g/m^2)

Season	Life form	Average±SE	SD.	Max	Min (excluding 0)
Dry season (944 sub-plots)	Ruzi	16.26±0.62	19.03	119.2	0.4
	Grass	5.01±0.48	14.61	142	0.4
	Forb	2.75±0.23	7.14	104.4	0.4
	Shrub	0.39±0.1	3.19	67.2	0.8
Wet season (2,080 sub-plots)	Ruzi	73.93±1.44	65.9	354	0.4
	Grass	11.69±0.57	26.17	317.2	0.4
	Forb	22.97±0.91	41.68	588.8	0.4
	Shrub	4.41±0.52	23.75	730.8	0.4

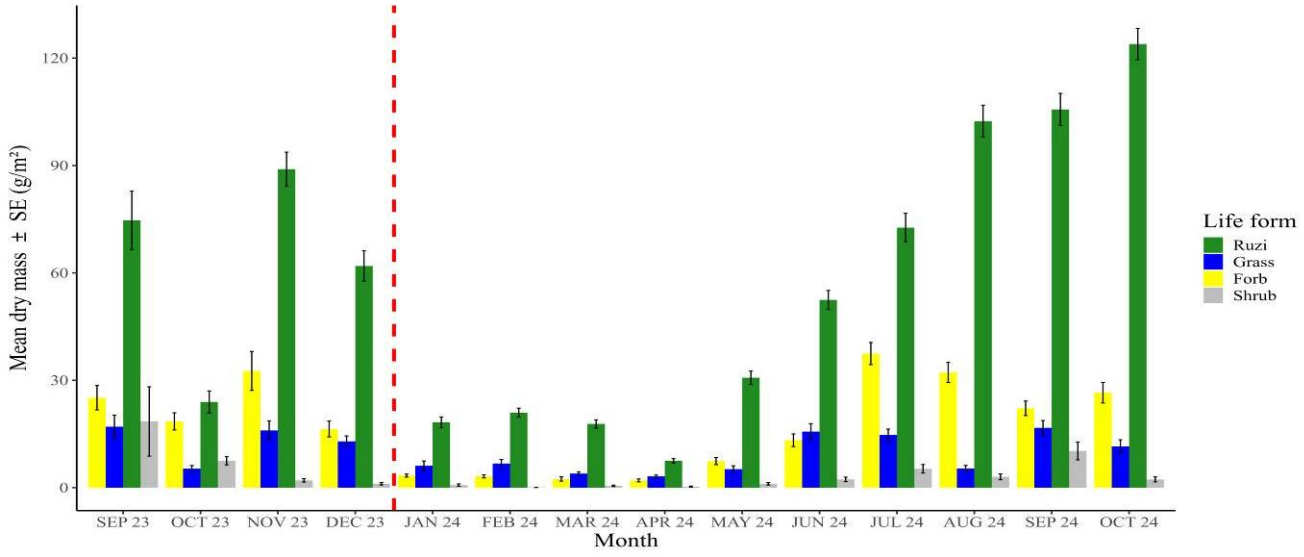

Figure 7. Mean dry biomass with error bars for each life form across the sampling period. The dashed line separates the years 2023 and 2024

Digital image-based classification via CNN

In total, 3,004 digital images were collected and used as input to the CORN model. The confusion matrix in Figure 8 indicates that the CNN successfully classified target biomass grass from digital images, even in complex backgrounds containing unwanted plant life forms and bare soil. The model classified biomass classes with an MAE of±0.351 classes; it showed good estimation performance in low and high biomass classes but exhibited lower accuracy in the middle class (Figure 8).

Fine-tuning to UAV imagery

In total, 21 areas were captured by UAV. From these, 1,710 grids (lacking tree cover within Sentinel-2 grid cells) were selected and predicted for biomass at a resolution of 50 × 50 cm. The model performance based on UAV imagery showed an MAE of ±0.340 classes and exhibited a trend similar to that observed with digital images. Therefore, the model was able to effectively bridge digital images to UAV imagery (Figure 9).

Grass biomass distribution modeling based on Sentinel-2

The optimal random forest model (ntree = 700 and mtry = 14) was used to predict spatiotemporal variability in grass biomass throughout the year across the study site. Figure 10 indicates good performance in predicting grass biomass, based on the linear relationship between grass biomass derived from UAV imagery and that estimated from Sentinel-2 imagery. Low biomass values (0-75 g/m^2) and high values (100-140 g/m^2) were predicted with good estimation accuracy, whereas intermediate biomass values showed fluctuating predictions with a tendency toward overestimation (Figure 10).

Table 3 presents model performance by month. The model showed good estimation during the early driest month (March), early wet season (May-June), and late wet season (October). In contrast, model performance was fair during the driest month (April) and parts of the wet season during growth period (August-September).

Monthly spatiotemporal variation in biomass distribution and its uncertainty

The biomass distribution was computed across the year 2024 using available Sentinel-2 data. Estimates from June to September were excluded due to persistent cloud cover during the wet season. Figures 11 and 12 show temporal variation in grass biomass across the year, following a trend similar to observed data. Grass biomass was lowest during the dry season; minimum values were recorded in March and April at 34.82±0.09 and 35.09±0.09 g/m^2, respectively. The grass, predominantly ruzi, began its growth with steadily increasing productivity, reaching peak values in October and November at 106.89±0.38 and 110.03±0.32 g/m^2, respectively. Biomass sharply declined in December. The average estimated biomass closely matched the observed values. The spatial pattern was evenly distributed across the grassland. In some areas (Figure 11, orange boxes), biomass was lower than in surrounding areas during the wet season.

The temporal pattern of uncertainty in biomass estimation varied across the season (Figure 13). The uncertainty generally followed a trend similar to the biomass values; in other words, low biomass values were associated with high uncertainty. Most areas showed uncertainty levels between 20-40% CV during the dry season (average 23.14%), while the CV steadily decreased during the wet season (average 17.52%), reaching its lowest point in November (average 11.11%), before sharply increasing again in December. The maximum average CV value was recorded in May (27.55%), corresponding to the transition season and plant growth stage. Meanwhile, the spatial pattern was unevenly distributed across the grassland.

Table 3. Upscaling model performance by month. Best performance coincided with peak biomass periods in October and transition season in May

Month	Number of test samples	RMSE (g/m^2)	NRMSE (%)
MAR	44	4.30	12.12
APR	35	7.13	19.48
MAY	33	4.79	10.54
JUN	4	10.54	14.06
AUG	21	14.24	18.87
SEP	4	18.46	18.32
OCT	33	10.03	8.49

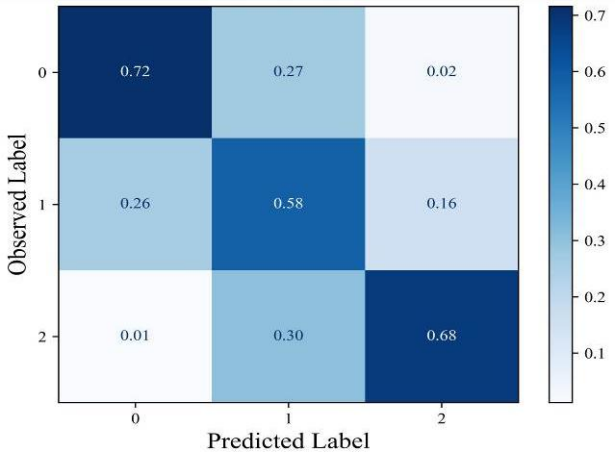

Figure 8. Normalized confusion matrix illustrating the classification performance of the CNN model based on digital images

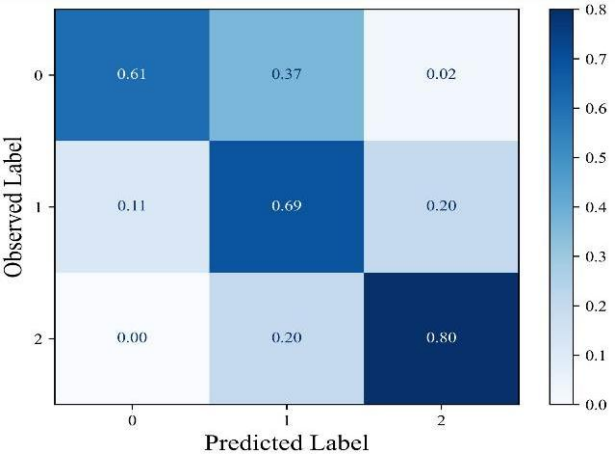

Figure 9. Normalized confusion matrix illustrating the classification performance of the CNN model based on UAV imagery

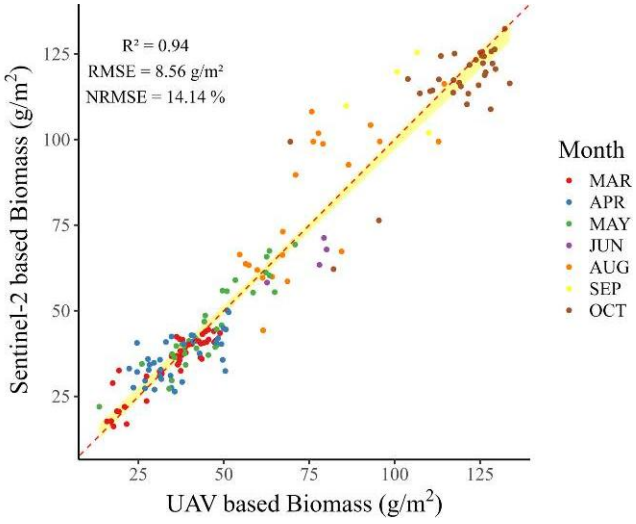

Figure 10. Predicted grass biomass based on Sentinel-2 vs UAV. The dashed red line represents the ideal fit, and the yellow ribbon represents the 95% confidence interval

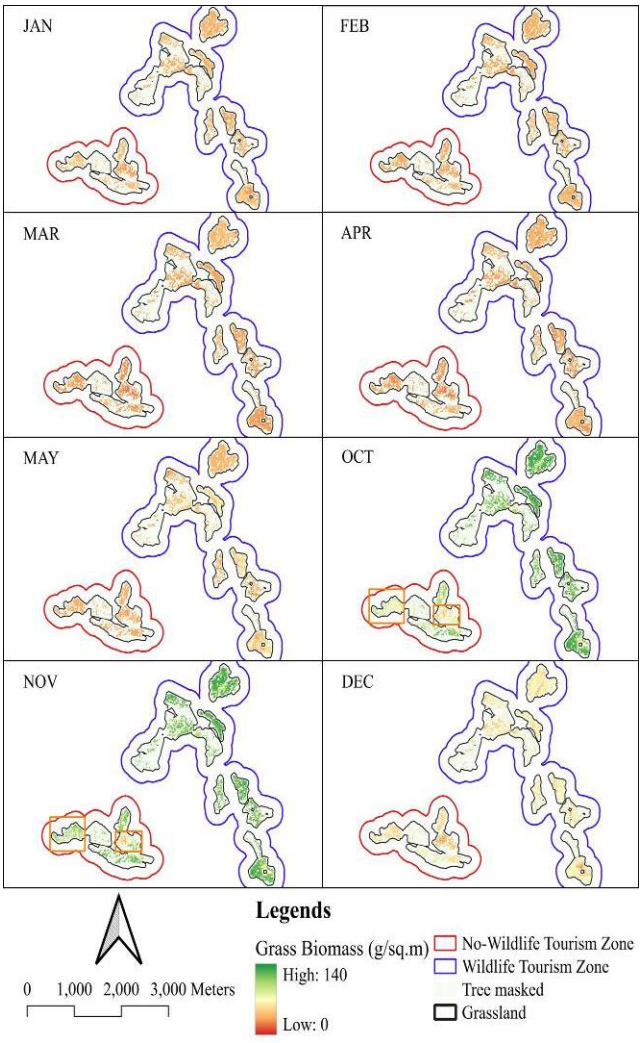

Figure 11. Spatiotemporal of grass biomass distribution based on Sentinel-2 throughout the year 2024. The orange boxes in October and November indicate areas where biomass was underestimated

Monthly carrying capacity of grassland

The results of grassland yield show the lowest dry mass production in March and April, with approximately 66.78-67.45 tons/month, and the highest yields in November, with approximately 210.86-213.26 tons/month. Monthly CC estimates for gaur indicate that the grassland could support the highest number of individuals in November and October, with approximately 284 to 296 gaur. In contrast, during the dry season, the grassland could support around 93 to 110 gaur (Table 4). The RSD reflects the monthly status of the grassland. Most months were categorized as "seriously overexploited" (December to January); only during the wet season (July-November), was categorized as "unexploited" or "normal" status based on observed biomass trends (Figure 12 and Table 4).

Discussion

Dynamic ruzi grass productivity and carrying capacity

Figures 7, 11, and 12 illustrate the dynamics of grass biomass, both observed and predicted, across the study site, revealing large fluctuations across seasons and within months. Several factors contribute to this variability. First, seasonal fluctuations are driven by precipitation patterns (Umuhoza et al. 2021), such that rainfall is high during the wet season and low in summer. These results suggest that water availability acts as a limiting factor for ruzi grass growth (Department of Livestock Development 2002; Dos Reis et al. 2020). Second, the model-based approach introduces intra-month variability because sampling is tied to model performance, leading to uncertainty in observed biomass. Third, significant differences between observed and predicted values occur during the dry season (Figure 12), with overestimation in low biomass areas (Class 0 biomass range: 0.00-24.80 g/m^2). In contrast, no significant differences were found during the wet season.

Dos Reis et al. (2020) reported an average of 202.19 g/m^2 during the growing season under rotational grazing, whereas the Department of Livestock Development (2002) reported average dry mass yields of 1,250-1,562.5 g/m^2. These discrepancies indicate overgrazing in this grassland, likely due to open grazing management (Abdelsalam et al. 2017). This area also hosts the largest herd of gaur (>60 individuals) and shows the highest intensity of habitat use relative to other zones in the national park (Steinmetz et al. 2011; Tanasarnpaiboon 2016). Moreover, CC analysis indicates heavy overpopulation, with gaur numbers exceeding 100% of the CC during the dry season. These findings confirm that overgrazing and overpopulation have led to reduced productivity and degradation of the grassland (Menke and Bradford 1992; Umuhoza et al. 2021). However, the reference for the gaur population is almost over a decade old, and the population may have changed in the intervening years. This represents a source of uncertainty in the CC analysis. Although elephants were excluded from the CC analysis, even minimal grazing by elephants (or other herbivores) could contribute cumulative pressure on the grassland, leading to further overexploitation.

There have been many reports of low tiger abundance in the park, with a relative abundance of 1.07% and a density of 0.36 individuals per 100 km² (Steinmetz et al. 2012; National Parks Research Center (Petchburi) 2018; Duangchantrasiri 2022). The absence of tigers is a contributing factor to gaur

overpopulation (Steinmetz et al. 2009). Gaur are prey for large predators such as tigers, leopards, and dholes (Karanth and Sunquist 1995; Ngoprasert et al. 2012), but only tigers are known to kill adult gaur (Rabinowitz 1989; Karanth and Sunquist 1995). The implementation of the Spatial Monitoring and Reporting Tool (SMART) has strengthened law enforcement and reduced hunting pressure, contributing to gaur population recovery (Steinmetz et al. 2010, 2014).

Pastor et al. (1997) noted that spatial heterogeneity, including resource distribution, plant tissue chemistry, and animal movement, affects population dynamics and CC. However, in this study, the environment was relatively homogeneous in terms of physical variables and plant cover, minimizing such effects. The biomass distribution model was constrained by canopy cover and could only predict biomass accurately in open areas, leading to uncertainty in yield estimates. Although gaur were distributed throughout the grassland, current population density data are unavailable.

Preliminary experiments showed no evidence of ruzi grass growth outside cultivated open areas after approximately 20 years of sowing; all 26 sampling plots outside cultivated zones showed no presence of ruzi grass. Although there are minimal direct data regarding *B. ruziziensis* invasiveness, related species such as *Brachiaria brizantha* (A.Rich.) Stapf and *Brachiaria decumbens* Stapf have shown invasive traits such as aggressive competition, high growth rates, reduced native species composition, and broad adaptability (Skerman and Riveros 1990; Department of Livestock Development 2002; Ferreira et al. 2016; Vieira et al. 2019; Diamante et al. 2020; Masters et al. 2024). These species also produce phytotoxins to enhance competitiveness (Barbosa et al. 2008). However, due to high light demand, ruzi grass is among the least shade-tolerant species (Wong et al. 1985; Odum and Barrett 2007), making it non-invasive in dense forest. Canopy shading at forest edges acts as a natural barrier against grass invasion (Foxcroft et al. 2011; Ferreira et al. 2016; Lopes et al. 2023).

Historically, before ruzi grass cultivation, the grassland was dominated by invasive species such as *Imperata cylindrica* (L.) Raeusch., *Chromolaena odorata* (L.) R.M.King & H.Rob., and *Pennisetum polystachion* (L.) Schult. (Srikrachang and Srikosamatara 2005). These species are not consumed by herbivores and are considered highly invasive in Thailand's protected areas (Forest and Plant Conservation Research Office 2013). Therefore, cultivation of ruzi grassland is more beneficial than allowing natural regeneration.

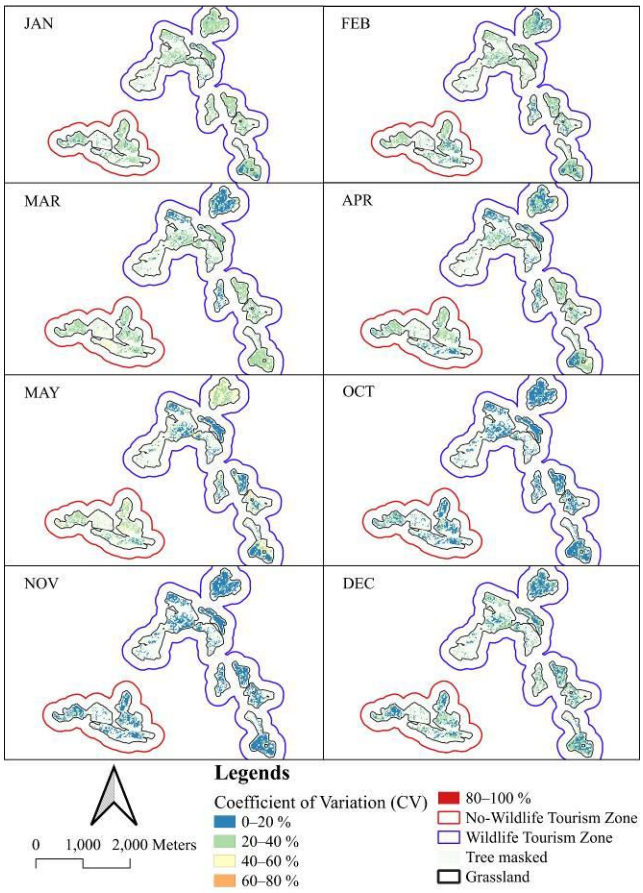

Figure 13. Monthly uncertainty maps for biomass estimation across the year 2024 based on optimal RF model

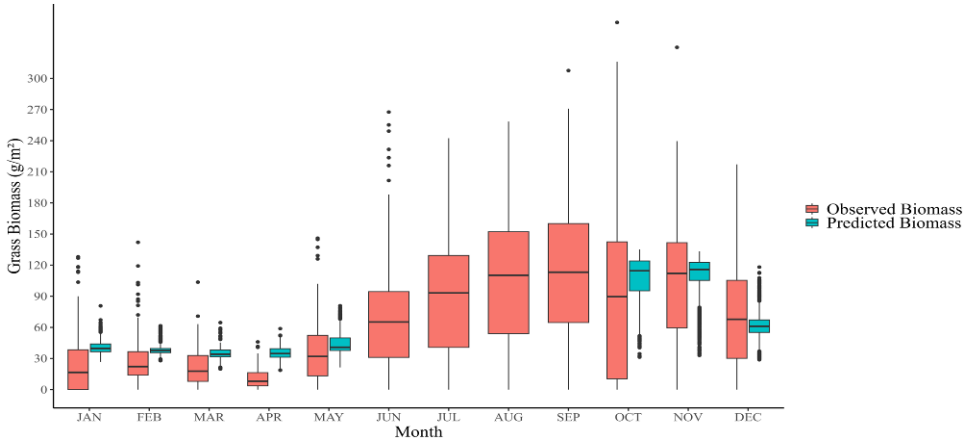

Figure 12. Predicted grass biomass based on Sentinel-2 across the year 2024, compared with observed biomass data collected during 2023-2024. Estimated biomass from June to September were excluded due to persistent cloud cover during the wet season

Table 4. Monthly carrying capacity and Relative Stocking Density (RSD) of gaurs in the grassland, based on monthly grass biomass estimates from the satellite-level model at the 95% Confidence Interval (CI). The grassland could support the highest number of gaurs in November and October, and lowest in March and April

Month	Grass biomass at 95% CI (g/m^2)	Grass biomass at 95% CI (tons/month)	Gaur intake per month (kg/individual /month)	Gaur population in central of Kui Buri National Park	Number of gaurs (individuals/ month)	Relative Stocking Density (RSD)
JAN	40.74±0.21	78.11-78.94	720	198-239 gaur (overall in the park) (Tanasarnpaiboon 2016)	108-110	2.00
FEB	37.89±0.13	72.77-73.29			101-102	2.15
MAR	34.82±0.17	66.78-67.45			93-94	2.34
APR	35.09±0.18	67.29-67.97			93-94	2.34
MAY	44.12±0.33	84.39-85.66			117-119	1.85
OCT	106.89±0.74	204.58-207.42			284-288	0.76
NOV	110.03±0.62	210.86-213.26			293-296	0.74
DEC	60.88±0.37	116.62-118.03			162-164	1.34

Ground biomass classification

The overall performance of biomass class classification was fair. Classification errors were limited to adjacent classes (±1 class), which aligns with the concept of ordinal classification proposed by Cao et al. (2020) and Shi et al. (2023). In general, deep learning performs less effectively with limited training datasets but achieves higher accuracy when larger datasets are available, as noted by Marcus (2018) and Lukas et al. (2023).

This moderate accuracy can be attributed to two primary factors. First, uncertainty in environmental conditions and the image capture process played a role (Stockman and Shapiro 2001). Due to difficulties accessing the study site, a tripod was not used to collect images; some photographs were thus taken at non-parallel angles. As illustrated in Figure 5, this approach led to shadows from surrounding trees in certain images, blurriness from out-of-focus captures, and uneven lighting conditions caused by variable image capture times (between 10:00 a.m. and 4:30 p.m.). These issues were mitigated through image augmentation techniques, including shear transformation for misalignment, brightness adjustment for lighting variation, and Gaussian noise addition to help the model learn from imperfect data (Han et al. 2022).

Second, the nature of the input data itself contributed to classification errors. High background diversity, including forage life forms, grass litter, bare soil, and rocks, hindered accurate biomass estimation, especially in Class 1 classification. Class 2 showed the best performance because it was typically composed entirely of ruzi grass and other grass species. Class 0 predominantly consisted of forbs, shrubs, bare soil, or rock. Figure 14 illustrates object diversity within each class. Overestimation of Class 0 occurred in images containing grass litter and moderate weed cover, where biomass values were close to Class 1 (Q3 at 15.8 g/m^2). Correct Class 0 classification was associated with images dominated by bare soil, weeds, or very low biomass. Class 1 was overestimated in images containing diverse vegetation and biomass values that approached those of Class 2 (Q3 at 92.8 g/m^2), whereas underestimation occurred in images with sparse green biomass, grass litter, low weed density, and values near Class 0 (Q2 at 32.4 g/m^2). Accurate classification in Class 1 was most often observed for images with sparse weed cover. Class 2 underestimation was mainly due to the creeping growth habit and overlapping large leaves of ruzi grass at ground level, which made leaf shape difficult to detect in small pixel windows (Ma et al. 2019; Dos Reis et al. 2020; Masters et al. 2024), as shown in Figures 15-17.

Although previous studies have demonstrated strong CNN performance for biomass estimation using digital imagery or UAV RGB channels, they have typically relied on large datasets often containing more than 10,000 images. They have also utilized controlled conditions such as uniform cultivation in horticulture, livestock farms, or rice fields (Ma et al. 2019; Han et al. 2022; Nakajima et al. 2023). These datasets mainly contain the target species and bare soil, unlike the present study, which included non-target plants in naturally heterogeneous environments. Ma et al. (2017) noted that classification in complex landscapes using only RGB input is inherently more difficult. Hyperspectral sensors have been recommended to discriminate weed species (Li et al. 2021) but were not available in this study.

Additionally, the small image size reduced the ability of our model to discern leaf shape and life form. Ma et al. (2019), Jin et al. (2020) and Zhu et al. (2024) proposed including inputs such as canopy height and leaf area index to improve model accuracy; such inputs require LiDAR, which is costly and difficult to apply over large areas due to battery limitations. Digital cameras cannot provide these metrics.

Table 5 show preliminary experiments that greater image resolution improves biomass classification performance. These findings suggest that low-altitude UAV flights paired with high-resolution cameras represent an effective method to capture detailed image features and improve biomass class prediction in highly diverse forage environments.

Model performance bridging UAV imagery to Sentinel-2 imagery

This approach processed biomass estimation by bridging the ground scale to the satellite scale using UAV imagery, rather than directly modeling from ground to satellite scale. The overall performance of the bridging model was fair. The UAV-based model, which tended to overestimate Class 0 biomass, led to overestimation in the low biomass class (range: 0-24.80 g/m^2) during the March-April mapping period. It also produced fluctuating estimates in the middle biomass class during May-July and December-February, along with slight underestimation in the high

biomass class (during June-November (Figures 9-12). The wide biomass ranges in Class 0 and Class 1 contributed to substantial differences between observed and predicted values (Figure 12), resulting in overestimation during the dry season. Additionally, accuracy was insufficient in the driest month (April) and during the wet season (August and September) (Table 3).

One contributing factor was the uneven distribution of monthly UAV samples. UAV image capture was easier in the dry season than in the wet season, leading to a right-skewed sample distribution (12.76-52.78 g/m^2), with a concentration of values in the higher biomass range (112.78-132.78 g/m^2) and sparse representation in the intermediate range (52.78-112.78 g/m^2). This skew affected model accuracy, yielding high accuracy in the dry season and late wet season but low accuracy in the early wet season and months with limited training data (June-September). To address these gaps in future work, data augmentation using the Synthetic Minority Over-sampling Technique for Regression with Gaussian Noise could be conducted (Branco et al. 2017). Several studies have shown that this technique improves model performance compared with the use of original data alone (Agrawal and Petersen 2021; De Santi et al. 2022; Arteaga et al. 2023).

Table 5. Preliminary experiments showed that greater image resolution improves biomass classification performance

Image resolution (pixels)	Biomass classes	MAE	Classification accuracies (respectively)
224 ×224 (VGG19 as the backbone)	5	0.463	85%, 46%, 47%, 46%, and 77%
150 × 150	5	0.475	86%, 33%, 45%, 62%, and 65%
100 × 100	4	0.359	68%, 57%, 45%, and 87%
76 × 76	4	0.421	82%, 46%, 24%, and 90%
50 × 50	3	0.352	71%, 48%, and 85%

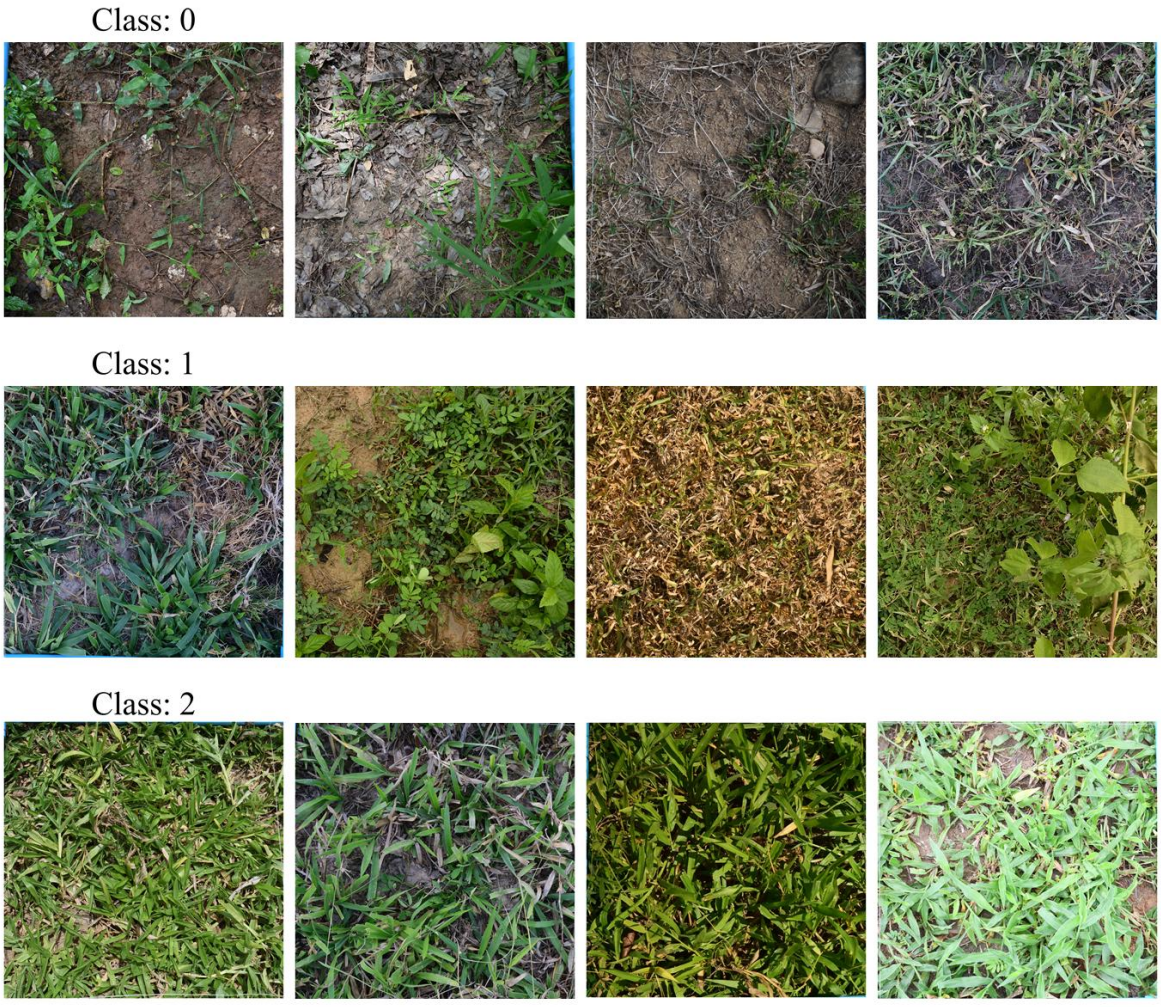

Figure 14. Characteristic and features of digital images for each grass biomass class

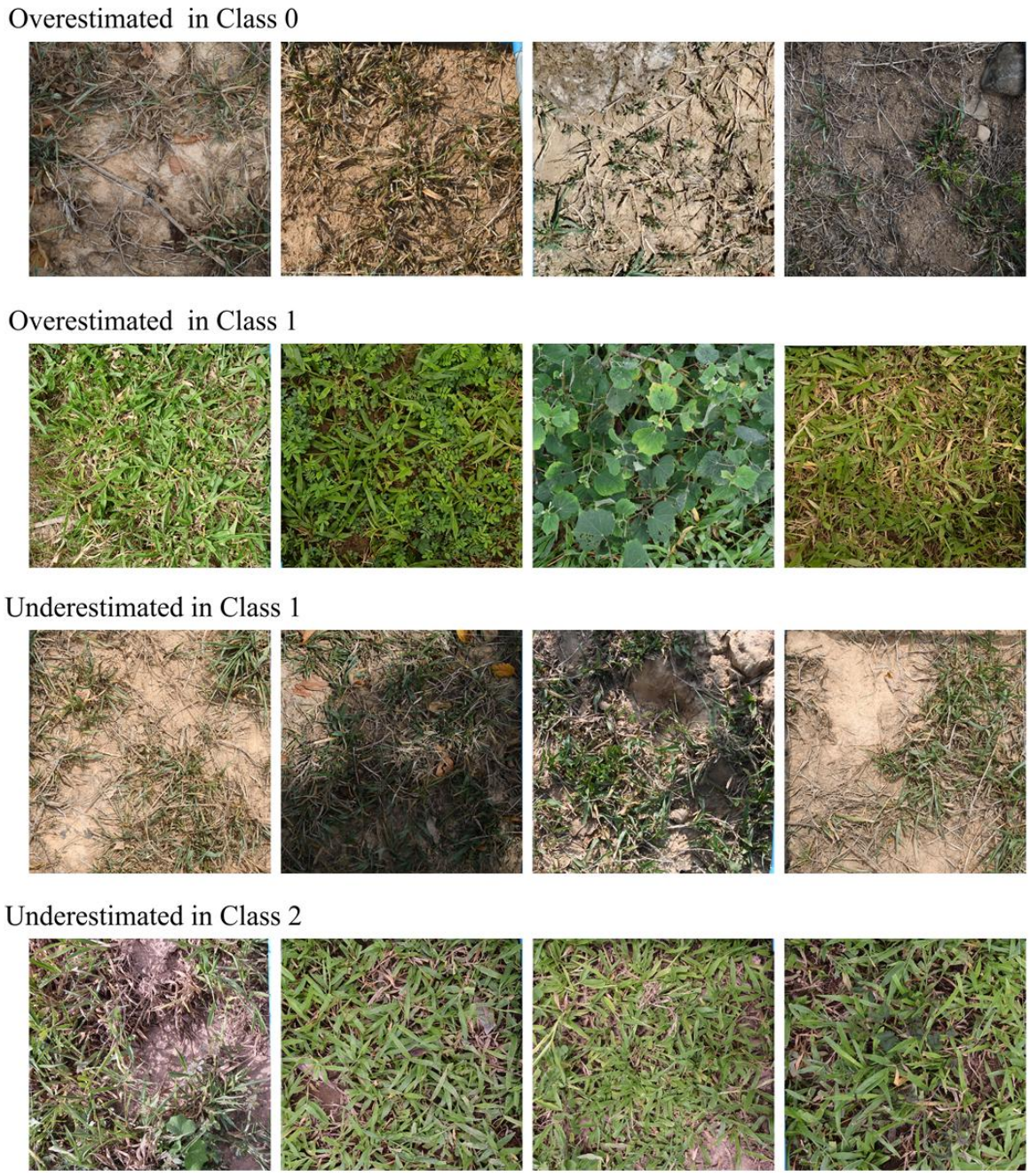

Figure 15. Characteristics and features of misclassified digital image in the ground-scale model

In areas predicted to have low biomass during the wet season, underestimation was observed (see orange boxes in October and November in Figure 11). This finding can be explained by the presence of dense weeds at various growth stages, which contributed to forage heterogeneity and overshadowed the grass. Furthermore, conventional machine learning models require one-dimensional vector inputs, which tend to underperform in heterogeneous environments relative to CNNs that can process two-dimensional or three-dimensional structured data (Schreiber et al. 2022). These areas can be flagged as top-priority zones for management. Similar to many previous studies, biomass was used as an index for habitat management and coservation priority. In this context, forage biomass was considered a manageable factor for habitat improvement, meaning that areas with low biomass were identified as top-priority zones for management (Paansri et al. 2022). Similarly, areas with high forest carbon stock were considered as strictly protected zones, important for compensating greenhouse gas emissions and conserving biodiversity in tropical forest, which is positively correlated with biomass (Van Con et al. 2013; Morandi et al. 2020). In conservation zoning, Lesmerises et al. (2011) prioritized areas with dense forage biomass for the conservation food source of ungulates.

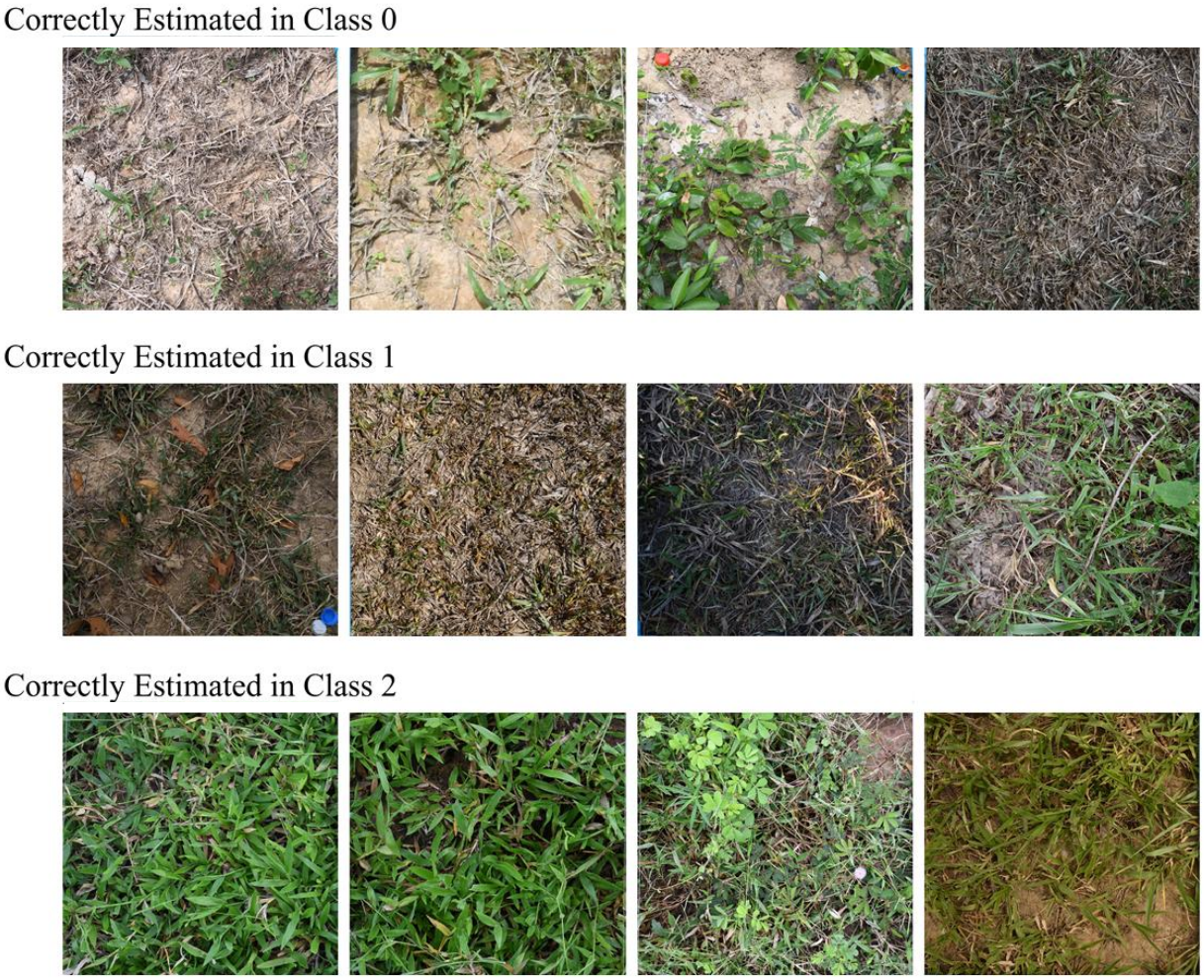

Figure 16. Characteristics and features of correctly classified digital images in the ground-scale model

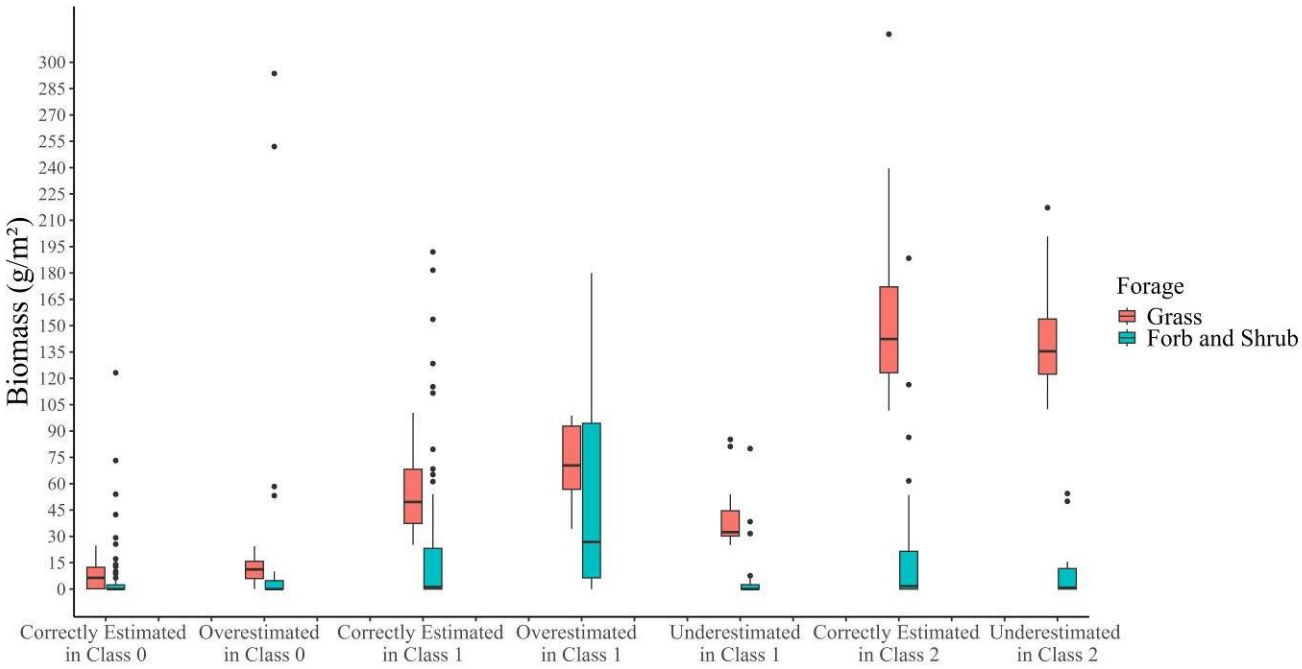

Figure 17. Characteristics of grass and weed biomass (forages and shrubs) in misclassified images

The combination of UAV and satellite imagery with CNN has been applied in various ways to estimate biomass. For example, Tao et al. (2024) used UAV imagery to extract individual tree biomass as ground sample biomass, while a CNN was employed to delineate the boundaries of target plant species with an accuracy of 1.0, which was crucial for biomass mapping based on satellite imagery (estimation via extreme gradient boosting model with R^2 = 0.669). Aydin and Setiawan (2024) extracted texture features by fusing UAV and satellite data to estimate forest carbon stocks using a CNN, achieving an accuracy of 0.71. Vawda et al. (2024) estimated grass biomass directly at satellite scale using CNN, based on multispectral data and VIs from Sentinel-2 imagery. Their model achieved an R^2 of 0.83, RMSE of 3.36 g/m^2, and NRMSE of 6.09%. In comparison, the bridging model in this study achieved an R^2 of 0.97, RMSE of 9.56 g/m^2, and NRMSE of 13.56%. Although our approach yielded slightly lower accuracy than the direct method, it offers the advantage of reducing sampling errors.

Limitations to ground-to-satellite biomass bridging

The experiment demonstrated the potential to bridge digital and UAV imagery (ground scale) to satellite scale using CNN models based on RGB inputs, rather than relying on conventional sampling methods that collect data from selected grid areas. However, several factors limited model performance.

First, the performance of the bridging model was highly dependent on the quality (image dimensions and resolution) and quantity (number of observations) of both digital and UAV imagery. Given that biomass estimates from these sources were used as training samples for the upscaling model, limitations in RGB-only input data constrained CNN performance. Poor-quality ground samples contributed to a wide range of biomass class predictions, resulting in overestimation during the dry season—despite good performance in estimating low biomass at the satellite scale. To address these problem, low-altitude UAV flights paired with high-resolution cameras represent an effective method to capture detailed image features and improve biomass class prediction in highly diverse forage environments and enhancing accuracy within a narrow range of biomass classes predictions (Table 5). Increasing the number of observations of both digital and UAV imagery could further improve model performance.

Second, coregistration errors between UAV and Sentinel-2 data (Diack et al. 2024) introduced spatial mismatches. These errors were primarily caused by GNSS positioning uncertainties in both UAV and Sentinel-2 datasets, leading to cases where UAV imagery (50 × 50 cm resolution) did not align with Sentinel-2 grid cells. However, very few studies have considered this problem. Recently, Gränzig et al. (2021) proposed new approach to reducing this the spatial shift.

Third, leaf overlapping and weed cover during late growth stages was a major source of underestimation and overderestimation, respectively. Canopy height and hyperspectral data could help mitigate this issue (Ma et al. 2019; Li et al. 2021), but such solutions are only applicable to UAV imagery at the ground scale.

Finally, the availability of Sentinel-2 data was limited by persistent cloud cover during the wet season, including the study site (May to December). This availability issue substantially reduced the frequency of cloud-free imagery, limiting biomass estimation and monitoring during key growth periods as well as annual grassland assessments. Additionally, this issue resulted in imagery being acquired far from the field observation dates, causing discrepancies between the derived variables and field observations, which led to inaccurate biomass estimation.

Application for grassland management and future directions

The present approach requires only cloud-free Sentinel-2 data for grass biomass monitoring. Therefore, biomass estimates can be continuously updated on any day that Sentinel-2 imagery is captured over the grassland. Furthermore, this approach can be applied to monitor the invasiveness of ruzi grass in areas beyond cultivation, as well as for spatial carrying capacity analysis, provided there is sufficient data on spatial wildlife density (Gränzig et al. 2021; Piipponen et al. 2022). GEE provides free, near-real-time satellite imagery, including Sentinel-2 data with a 5-day revisit interval. Earth Engine Apps are publicly accessible user interfaces for interacting with GEE analyses. The RF model developed in this study can be integrated into Earth Engine Apps to provide near-real-time insights into grass biomass dynamics.

This platform enables prioritization of grassland management without requiring field access. Areas predicted to have low grass biomass, often characterized by high weed cover or bare soil, can be flagged as top-priority zones for intervention. Additionally, Earth Engine Apps are web-based and offer a user-friendly interface for data analysis and visualization, making them accessible to national park officers without requiring specialized software or GEE accounts (Parracciani et al. 2024; Puspitasari et al. 2024). Future work should focus on developing and deploying such applications.

The results of the grassland CC analysis indicated that the area is currently supporting an overpopulation of wildlife. The degradation of grassland is a critical factor contributing to wildlife overpopulation. To mitigate this overpopulation, especially in dry season, water resource management strategies should be implemented to utilize all 12 reservoirs and numerous ponds within the restoration area, ensuring that water flows into the grassland, where water availability acts as a limiting factor for ruzi grass growth (Department of Livestock Development 2002; Srikrachang and Srikosamatara 2005; Dos Reis et al. 2020). Nowaday, only annual sowing of ruzi seeds is practiced to support regeneration and mitigates trampling effects (DNP 2022). Pasture management practices such as grazing rotation management should be integrated to improve wildlife habitat (Vavra 2005). To implement grazing rotation on the grassland, the two grassland management zone should be fenced. Tekletsadik et al. (2004) reported that in the dry season, lax cutting of ruzi grass at stubble

heights of 20 cm above the ground and cutting every month produced higher dry matter yield and crude protein content than close cutting at stubble heights of 5 cm above the ground and cut every three months or only once in April. Moreover, Neutral Detergent Fiber (NDF) and Acid Detergent Fiber (ADF) contents tended to be higher under lax cutting than close cutting in both seasons. Therefore, to implement grazing rotation, one zone was grazed at stubble heights of 20 cm above the ground while another zone was left ungrazed. Grazing rotation occurred every month, meaning that in the following month, the zone that was ungrazed in the previous month was grazed, while the previously grazed zone was allowed to recover. Wildlife tourism zones were moved according to the grazing rotation schedule. These strategies aim to maintaining grassland for provides year-round resources for wildlife, increase the carrying capacity, and enhance the potetial yields of the grassland efforts that reduce gaurs and elephants crop raiding (Prayoon et al. 2024).

In summary, this study proposes a novel approach to bridging the gap between ground-scale and satellite-scale biomass estimation, which reduces sampling errors. The method integrates digital images, UAV imagery, and Sentinel-2 data through an ordinal regression CNN model. The ground-scale model showed fair performance, whereas the satellite-scale model performed well. Future work should incorporate larger training datasets focused on middle biomass values with heterogeneous backgrounds and utilize higher-resolution UAV imagery to improve ground-scale model accuracy. The primary objective of this study—to demonstrate the feasibility of bridging ground and satellite scales—was successfully achieved. The estimated grass biomass was used in CC analysis, which revealed clear evidence of overgrazing and gaur overpopulation in the grasslands. To address this issue, grazing rotation and water resource management was recommended as strategies to rehabilitate degraded grasslands, ensure year-round forage availability for wildlife, and improve potential the grassland's productivity, thereby mitigating human-wildlife conflict in the buffer zone of Kui Buri National Park.

ACKNOWLEDGEMENTS

The research was supported by Kasetsart University from Thailand through the "Precision Wildlife Management for Kui Buri National Park" project. This research is funded by Kasetsart University through the Graduate School Fellowship Program. We would like to thank everyone who is involved in this research. Special thanks to the undergraduate and graduate students from the Faculty of Forestry for their assistance on field data collection. We also thank Kui Buri National Park officers and the Department of National Parks, Wildlife and Plant Conservation for granting permission and providing support during fieldwork. Lastly, we are grateful for the support received from the Faculty of Forestry, Kasetsart University. The data, modeling code, and image processing procedures used in this study are available upon request from the corresponding author.

REFERENCES

Abdelsalam MI, Abdalla NI, Abdelkreim M, Ibrahim ME, Mohammed MM. 2017. The impact of continuous grazing on natural rangeland in Alazzazah area-Blue Nile State, Sudan. J Rangel Sci 7 (4): 309-315.

Agrawal A, Petersen MR. 2021. Detecting arsenic contamination using satellite imagery and machine learning. Toxics 9 (12): 333. DOI: 10.3390/toxics9120333.

Aiello S, Eckstrand E, Fu A, Landry M, Aboyoun P. 2016. Machine Learning with R and H2O. H2O.ai, California.

Amorim JGA, Schreiber LV, de Souza MRQ, Negreiros M, Susin A, Bredemeier C, Trentin C, Vian AL, de Olivera Andrades-Filho C, Doering D, Parraga A. 2022. Biomass estimation of spring wheat with machine learning methods using UAV-based multispectral imaging. Intl J Remote Sens 43 (13): 4758-4773. DOI: 10.1080/01431161.2022.2107882.

Araza A, De Bruin S, Herold M et al. 2022. A comprehensive framework for assessing the accuracy and uncertainty of global above-ground biomass maps. Remote Sens Environ 272: 112917. DOI: 10.1016/j.rse.2022.112917.

Arteaga M, Gacto MJ, Galende M, Alcalá-Fdez J, Alcalá R. 2023. Enhancing soft computing techniques to actively address imbalanced regression problems. Expert Syst Appl 234: 121011. DOI: 10.1016/j.eswa.2023.121011.

Ashokkumar M, Swaminathan S, Nagarajan R, Desai AA. 2011. Distribution, ecology and conservation of the gaur (*Bos gaurus*, H. Smith, 1824). In: Gupta VK, Verma AK (eds). Animal Diversity, Natural History and Conservation. Daya Publishing House, New Delhi.

Aydin R, Setiawan EB. 2024. Estimating forest carbon stocks using CNN and vegetation texture features extracted from UAV and satellite data in Telkom University. J Ilmiah Teknik Elektro Komputer dan Informatika 10 (4): 976-991. DOI: 10.26555/jiteki.v10i4.30546.

Baccini A, Friedl MA, Woodcock CE, Zhu Z. 2007. Scaling field data to calibrate and validate moderate spatial resolution remote sensing models. Photogramm Eng Remote Sens 73 (8): 945-954. DOI: 10.14358/pers.73.8.945.

Bannari A, Asalhi H, Teillet PM. 2002. Transformed Difference Vegetation Index (TDVI) for vegetation cover mapping. In: Proceedings of the IEEE International Geoscience and Remote Sensing Symposium. Toronto, ON, Canada, 24-28 June 2002.

Barbosa EG, Pivello VR, Meirelles ST. 2008. Allelopathic evidence in *Brachiaria decumbens* and its potential to invade the Brazilian Cerrados. Braz Arch Biol Technol 51 (4): 825-831. DOI: 10.1590/S1516-89132008000400021.

Baskaran N, Balasubramanian M, Swaminathan S, Desai AA. 2010. Feeding ecology of the Asian elephant *Elephas maximus* Linnaeus in the Nilgiri Biosphere Reserve, Southern India. J Bombay Nat Hist Soc 107 (1): 3-13.

Beohar D, Rasool A. 2021. Handwritten digit recognition of MNIST dataset using deep learning state-of-the-art Artificial Neural Network (ANN) and Convolutional Neural Network (CNN). In: Proceeding of 021 International Conference on Emerging Smart Computing and Informatics (ESCI). Pune, India, 5-7 March 2021. DOI: 10.1109/esci50559.2021.9396870.

Bleich VC, Oehler MW, Kie JG. 2020. Managing rangelands for wildlife In: Silvy NJ (eds). The Wildlife Management Techniques Manual. Johns Hopkins University Press, Baltimore.

Boser BE, Guyon IM, Vapnik VN. 1992. A training algorithm for optimal margin classifiers. Proceedings of the Fifth Annual Workshop on Computational Learning Theory. ACM, New York, USA. DOI: 10.1145/130385.130401.

Boyd DS, Danson FM. 2005. Satellite remote sensing of forest resources: Three decades of research development. Prog Phys Geogr 29 (1): 1-26. DOI: 10.1191/0309133305pp432ra.

Branco P, Torgo L, Ribeiro RP. 2017. SMOGN: A pre-processing approach for imbalanced regression. Proceedings of the First International Workshop on Learning with Imbalanced Domains: Theory and Applications. PMLR, Skopje, Macedonia, 18-22 September 2017.

Breiman L. 2001. Random forests. Mach Learn 45: 5-32. DOI: 10.1023/A:1010933404324.
Cao W, Mirjalili V, Raschka S. 2020. Rank consistent ordinal regression for neural networks with application to age estimation. Pattern Recognit Lett 140: 325-331. DOI: 10.1016/j.patrec.2020.11.008.
Cappai MG, Aboling S. 2020. Toxic or harmful components of aromatic plants in animal nutrition. In: Florou-Paneri P, Christaki E, Giannenas I (eds). Feed Additives: Aromatic Plants and Herbs in Animal Nutrition and Health. Academic Press, Massachusetts.
Chauhan NK, Singh K. 2018. A review on conventional machine learning vs deep learning. In: 2018 International Conference on Computing, Power and Communication Technologies (GUCON). Greater Noida, India. DOI: 10.1109/gucon.2018.8675097.
Chehade AH, Abdallah N, Marion J-M, Oueidat M, Chauvet P. 2022. Lung and colon cancer classification using medical imaging: A feature engineering approach. Phys Eng Sci Med 45 (3): 729-746. DOI: 10.21203/rs.3.rs-1211832/v1.
Chen J, Deng X, Zhang L, Bai Z. 2006. Diet composition and foraging ecology of Asian elephants in Shangyong, Xishuangbanna, China. Acta Ecol Sin 26 (2): 309-316. DOI: 10.1016/S1872-2032(06)60006-1.
Chen JM. 1996. Evaluation of vegetation indices and a modified simple ratio for boreal applications. Can J Remote Sens 22(3): 229-242. DOI: 10.1080/07038992.1996.10855178.
Cinar S, Abdullayev A, Esenov N, Karadag Y. 2020. Determination of botanical composition, hay yield and forage quality of some natural rangelands in kyrgyzstan's chuy region. Appl Ecol Environ Res 18 (1): 401-416. DOI: 10.15666/aeer/1801_401416.
Copernicus Data Space Ecosystem (CDSE). 2017. Sentinel-2. https://dataspace.copernicus.eu/data-collections/copernicus-sentinel-data/sentinel-2.
Cox DR. 1958. The regression analysis of binary sequences. J R Stat Soc Ser B Stat Method 20 (2): 215-232. DOI: 10.1111/j.2517-6161.1958.tb00292.x.
De Leeuw J, Rizayeva A, Namazov E, Bayramov E, Marshall MT, Etzold J, Neudert R. 2019. Application of the MODIS MOD 17 Net Primary Production product in grassland carrying capacity assessment. Intl J Appl Earth Obs Geoinform 78: 66-76. DOI: 10.1016/j.jag.2018.09.014.
De Santi NSM, Rodrigues NVN, Montero-Dorta AD, Abramo LR, Tucci B, Artale MC. 2022. Mimicking the halo-galaxy connection using machine learning. Mon Not R Astron Soc 514 (2): 2463-2478. DOI: 10.1093/mnras/stac1469.
Decitre O, Joyce KE. 2024. Using YOLOv5, SAHI, and GIS with drone mapping to detect giant clams on the Great Barrier Reef. Drones 8 (9): 458. DOI: 10.3390/drones8090458.
Dehni A, Lounis M. 2012. Remote sensing techniques for salt affected soil mapping: Application to the Oran Region of Algeria. Procedia Eng 33: 188-198. DOI: 10.1016/j.proeng.2012.01.1193.
Department of Livestock Development. 2002. Ruzi Grass. The Agricultural Co-Operative Federation of Thailand, Bangkok. [Thai]
Department of National Parks, Wildlife and Plant Conservation (DNP). 2022. Action plan for human–elephant conflict mitigation in Kui Buri National Park, Prachuap Khiri Khan Province 2022–2027. Bangkok, Thailand: Ministry of Natural Resources and Environment. [Thai]
Diack I, Diene SM, Louise L et al. 2024. Combining UAV and Sentinel-2 imagery for estimating Millet FCover in a heterogeneous agricultural landscape of Senegal. IEEE J Sel Top Appl Earth Obs Remote Sens 17: 7305-7322. DOI: 10.1109/jstars.2024.3373508.
Diamante NA, Fabrin TM, Silveira MJ, de Oliveira AV, Thomaz SM, Prioli SMAP, Prioli AJ. 2020. Molecular analysis of the invasive populations of *Urochloa* (Poaceae) in a large Neotropical reservoir. Aquat Bot 161: 103183. DOI: 10.1016/j.aquabot.2019.103183.
DJI. 2025. DJI Terra. DJI, Shenzhen. Available online: https://www.dji.com/ (accessed on 15 January 2025).
Dong J, Hu SX. 1997. The progress and prospects of neural network research. Inform Control 26 (5): 360-368.
Dong L, Du H, Han N, Li X, Zhu D, Mao F, Zhang M, Zheng J, Liu H, Huang Z, He S. 2020. Application of convolutional neural network on Lei bamboo Above-Ground-Biomass (AGB) estimation using Worldview-2. Remote Sens 12 (6): 958. DOI: 10.3390/rs12060958.
Dong Y, Yan H-M, Du W-P, Hu Y-F. 2019. Spatio-temporal analysis of grassland carrying capacity in Mongolian Plateau based on supply-consumption relationship. J Nat Resour 34 (5): 1093-1107. DOI: 10.31497/zrzyxb.20190515.
Dos Reis AA, Werner JPS, Silva BC, Figueiredo GKDA, Antunes JFG, Esquerdo JCDM, Coutinho AC, Lamparelli RAC, Rocha JV, Magalhães PSG. 2020. Monitoring pasture aboveground biomass and canopy height in an integrated crop-livestock system using textural information from PlanetScope imagery. Remote Sens 12 (16): 2534. DOI: 10.3390/rs12162534.
Duangchantrasiri S. 2022. Tiger population assessment in the wild of Thailand, 2022. Wildl Yearb 20: 135-142. [Thai]
European Space Agency (ESA). 2014. Sentinel-2 Missions—Sentinel Online. ESA, Paris, France.
Ferreira LV, Parolin P, Matos DCL, Cunha DA, Chaves PP, Neckel SO. 2016. The effect of exotic grass *Urochloa decumbens* (Stapf) R.D. Webster (Poaceae) in the reduction of species richness and change of floristic composition of natural regeneration in the Floresta Nacional de Carajás, Brazil. An Acad Bras Cienc 88: 589-597. DOI: 10.1590/0001-3765201620150121.
Forest and Plant Conservation Research Office. 2013. Invasive Plants in Protected Area. The Agricultural Co-Operative Federation of Thailand, Bangkok. [Thai]
Foxcroft LC, Jarošík V, Pyšek P, Richardson DM, Rouget M. 2011. Protected-area boundaries as filters of plant invasions. Conserv Biol 25 (2): 400-405. DOI: 10.1111/j.1523-1739.2010.01617.x.
Frick H, Chow F, Kuhn M, Mahoney M, Silge J, Wickham H. 2025. Rsample: General Resampling Infrastructure. R package version 1.3.0. https://github.com/tidymodels/rsample, https://rsample.tidymodels.org.
Gao J, Liao W, Nuyttens D, Lootens P, Xue W, Alexandersson E, Pieters J. 2024. Cross-domain transfer learning for weed segmentation and mapping in precision farming using ground and UAV images. Expert Syst Appl 246: 122980. DOI: 10.1016/j.eswa.2023.122980.
Ge C, Zhang C, Zhang Y, Fan Z, Kong M, He W. 2024. Synergy of UAV-LiDAR data and multispectral remote sensing images for allometric estimation of phragmites australis aboveground biomass in coastal wetland. Remote Sens 16 (16): 3073. DOI: 10.3390/rs16163073.
Gitelson AA, Chivkunova OB, Merzlyak MN. 2009. Nondestructive estimation of anthocyanins and chlorophylls in anthocyanic leaves. Am J Bot 96 (10): 1861-1868. DOI: 10.3732/ajb.0800395.
Gitelson AA, Gritz Y, Merzlyak MN. 2003. Relationships between leaf chlorophyll content and spectral reflectance and algorithms for non-destructive chlorophyll assessment in higher plant leaves. J Plant Physiol 160 (3): 271-282. DOI: 10.1078/0176-1617-00887.
Gitelson AA, Kaufman YJ, Merzlyak MN. 1996. Use of a green channel in remote sensing of global vegetation from EOS-MODIS. Remote Sens Environ 58 (3): 289-298. DOI: 10.1016/S0034-4257(96)00072-7.
Gitelson AA, Merzlyak MN. 1994. Quantitative estimation of chlorophyll-a using reflectance spectra: Experiments with autumn chestnut and maple leaves. J Photochem Photobiol B: Biol 22 (3): 247-252. DOI: 10.1016/1011-1344(93)06963-4.
Gitelson AA, Merzlyak MN. 1997. Remote estimation of chlorophyll content in higher plant leaves. Intl J Remote Sens 18 (12): 2691-2697. DOI: 10.1080/014311697217558.
Gränzig T, Fassnacht FE, Kleinschmit B, Förster M. 2021. Mapping the fractional coverage of the invasive shrub Ulex europaeus with multi-temporal Sentinel-2 imagery utilizing UAV orthoimages and a new spatial optimization approach. Intl J Appl Earth Obs Geoinform 96: 102281. DOI: 10.1016/j.jag.2020.102281.
Han J, Shi L, Yang Q, Chen Z, Yu J, Zha Y. 2022. Rice yield estimation using a CNN-based image-driven data assimilation framework. Field Crops Res 288: 108693. DOI: 10.1016/j.fcr.2022.108693.
Hijmans R. 2025. terra: Spatial Data Analysis. R package version 1.8-44. https://rspatial.org/.
Himmelsbach W, Tagle MAG, Füldner K, Hoefle HH, Htun W. 2006. Food plants of captive elephants in the okkan reserved forest, Myanmar (Burma), Southeast Asia. Ecotropica 12: 15-26.
Holechek JL, Pieper RD, Herbel CH. 2010. Range Management: Principles and Practices. Prentice Hall, Las Cruces.
Holechek JL. 1984. Comparative contribution of grasses, forbs, and shrubs to the nutrition of range ungulates. Rangelands 6 (6): 261-263.
Huechacona-Ruiz AH, Dupuy JM, Schwartz NB, Powers JS, Reyes-García C, Tun-Dzul F, Hernández-Stefanoni JL. 2020. Mapping tree species deciduousness of tropical dry forests combining reflectance, spectral unmixing, and texture data from high-resolution imagery. Forests 11 (11): 1234. DOI: 10.3390/f11111234.
Huete AR. 1988. A Soil-Adjusted Vegetation Index (SAVI). Remote Sens Environ 25 (3): 295-309. DOI: 10.1016/0034-4257(88)90106-X.
Jensen RR, Hardin PJ, Yu G. 2009. Artificial neural networks and remote sensing. Geogr Compass 3 (2): 630-646. DOI: 10.1111/j.1749-8198.2008.00215.x.

Jin S, Su Y, Song S, Xu K, Hu T, Yang Q, Wu F, Xu G, Ma Q, Guan H, Pang S, Li Y, Guo Q. 2020. Non-destructive estimation of field maize biomass using terrestrial lidar: An evaluation from plot level to individual leaf level. Plant Methods 16: 69. DOI: 10.1186/s13007-020-00613-5.

Joshi R, Singh R. 2008. Feeding behaviour of wild Asian elephants (*Elephas maximus*) in the Rajaji National Park. J Am Sci 4 (2): 34-48.

Karanth KU, Sunquist ME. 1995. Prey selection by tiger, leopard and dhole in tropical forests. J Anim Ecol 439-450. DOI: 10.2307/5647.

Kattenborn T, Leitloff J, Schiefer F, Hinz S. 2021. Review on Convolutional Neural Networks (CNN) in vegetation remote sensing. ISPRS J Photogramm Remote Sens 173: 24-49. DOI: 10.1016/j.isprsjprs.2020.12.010.

Kaufman YJ, Tanré D. 1996. Strategy for direct and indirect methods for correcting the aerosol effect on remote sensing: From AVHRR to EOS-MODIS. Remote Sens Environ 55 (1): 65-79. DOI: 10.1016/0034-4257(95)00193-X.

Kim MS, Daughtry CST, Chappelle EW, Mcmurtrey JE. Walthall CL. 1994. The use of highspectral resolution bands for estimating absorbed photosynthetically active radiation (A par). In: Proceedings of the 6th International Symposium on Physical Measurements and Signatures in Remote Sensing, Val D'Isere, France, 17-21 January 1994.

Kingma DP, Ba J. 2014. Adam: A method for stochastic optimization. arXiv preprint arXiv:1412.6980. DOI: 10.48550/arXiv.1412.6980.

Kobayashi N, Tani H, Wang X, Sonobe R. 2020. Crop classification using spectral indices derived from Sentinel-2A imagery. J Inf Telecommun 4 (1): 67-90. DOI: 10.1080/24751839.2019.1694765.

Krizhevsky A, Sutskever I, Hinton GE. 2017. ImageNet classification with deep convolutional neural networks. Commun ACM 60 (6): 84-90. DOI: 10.1145/3065386.

Kui Buri National Park. 2003. Summary Results for the Year 2003. Kui Buri National Park, Thailand. [Thai]

Kumar L, Mutanga O. 2017. Remote sensing of above-ground biomass. Remote Sens 9 (9): 935. DOI: 10.3390/rs9090935.

Lesmerises R, Ouellet J-P, St-Laurent M-H. 2011. Assessing terrestrial lichen biomass using ecoforest maps: A suitable approach to plan conservation areas for forest-dwelling caribou. Can J For Res 41 (3): 632-642. DOI: 10.1139/X10-229.

Li Y, Al-Sarayreh M, Irie K, Hackell D, Bourdot G, Reis MM, Ghamkhar K. 2021. Identification of weeds based on hyperspectral imaging and machine learning. Front Plant Sci 11: 611622. DOI: 10.3389/fpls.2020.611622.

Liaw A, Wiener M. 2002. Classification and regression by randomForest. R News 2 (3): 18-22.

Lopes A, Demarchi LO, Piedade MTF, Schöngart J, Wittmann F, Munhoz CBR, Ferreira CS, Franco AC. 2023. Predicting the range expansion of invasive alien grasses under climate change in the Neotropics. Perspect Ecol Conserv 21 (2): 128-135. DOI: 10.1016/j.pecon.2023.02.005.

Lukas J, Kolb S, Heinbuch J, Willig L, Plankenbühler T, Müller D, Karl J. 2023. Image-based biomass characterization: Comparison of conventional image processing and a deep learning approach. Fuel 341: 127705. DOI: 10.1016/j.fuel.2023.127705.

Ma J, Du K, Zhang L, Zheng F, Chu J, Sun Z. 2017. A segmentation method for greenhouse vegetable foliar disease spots images using color information and region growing. Comput Electron Agric 142: 110-117. DOI: 10.1016/j.compag.2017.08.023.

Ma J, Li Y, Chen Y, Du K, Zheng F, Zhang L, Sun Z. 2019. Estimating above ground biomass of winter wheat at early growth stages using digital images and deep convolutional neural network. Eur J Agron 103: 117-129. DOI: 10.1016/j.eja.2018.12.004.

Mao P, Ding J, Jiang B, Qin L, Qiu GY. 2022. How can UAV bridge the gap between ground and satellite observations for quantifying the biomass of desert shrub community? ISPRS J Photogramm Remote Sens 192: 361-376. DOI: 10.1016/j.isprsjprs.2022.08.021.

Marcus G. 2018. Deep learning: A critical appraisal. arXiv preprint arXiv: 1801.00631. DOI: 10.48550/arXiv.1801.00631.

Mas JF, Flores JJ. 2008. The application of artificial neural networks to the analysis of remotely sensed data. Intl J Remote Sens 29 (3): 617-663. DOI: 10.1080/01431160701352154.

Masters LE, Tomaszewska P, Schwarzacher T, Hackel J, Zuntini AR, Heslop-Harrison P, Vorontsova MS. 2024. Phylogenomic analysis reveals five independently evolved African forage grass clades in the genus *Urochloa*. Ann Bot 133 (5-6): 725-742. DOI: 10.1093/aob/mcae022.

Menke J, Bradford GE. 1992. Rangelands. Agric Ecosyst Environ 42 (1-2): 141-163. DOI: 10.1016/0167-8809(92)90024-6.

Morandi PS, Marimon BS, Marimon-Junior BH et al. 2020. Tree diversity and above-ground biomass in the South America Cerrado biome and their conservation implications. Biodivers Conserv 29: 1519-1536. DOI: 10.1007/s10531-018-1589-8.

Nakajima K, Tanaka Y, Katsura K, Yamaguchi T, Watanabe T, Shiraiwa T. 2023. Biomass estimation of World rice (*Oryza sativa* L.) core collection based on the convolutional neural network and digital images of canopy. Plant Prod Sci 26 (2): 187-196. DOI: 10.1080/1343943X.2023.2210767.

Nargesian F, Samulowitz H, Khurana U, Khalil EB, Turaga D. 2017. Learning feature engineering for classification. Proceedings of the Twenty-Sixth International Joint Conference on Artificial Intelligence. DOI: 10.24963/ijcai.2017/352.

National Parks Research Center (Petchburi). 2018. Biodiversity Report of Wildlife in the ASEAN Heritage Site: Kui Buri National Park, Prachuap Khiri Khan Province. Petchburi, National Parks Research Center, Department of National Parks, Wildlife and Plant Conservation. [Thai]

Ngoprasert D, Lynam AJ, Sukmasuang R et al. 2012. Occurrence of three felids across a network of protected areas in Thailand: Prey, intraguild, and habitat associations. Biotropica 44 (6): 810-817. DOI: 10.1111/j.1744-7429.2012.00878.x.

Niu X, Chen B, Sun W, Feng T, Yang X, Liu Y, Liu W, Fu B. 2024. Estimation of coastal wetland vegetation aboveground biomass by integrating UAV and satellite remote sensing data. Remote Sens 16 (15): 2760. DOI: 10.3390/rs16152760.

Odum EP, Barrett GW. 2007. Fundamentos de Ecologia. Thomson Learning, São Paulo, Brazil. [Spanish]

Paansri P, Sangprom N, Suksavate W, Chaiyes A, Duengkae P. 2021. Spatial modeling of forage crops for tiger prey species in the area surrounding highway 304 in the Dong Phayayen-Khao Yai Forest complex. Environ Nat Resour J 19 (3): 220-229. DOI: 10.32526/ennrj/19/2020234.

Paansri P, Suksavate W, Chaiyes A, Chanteap P, Duengkae P. 2022. Use of bayesian, lasso binary quantile regression to identify suitable habitat for tiger prey species in Thap Lan National Park, Eastern Thailand. Environ Nat Resour 20 (3): 266-278. DOI: 10.32526/ennrj/20/202100244.

Parr JWK, Jitvijak S, Saranet S, Buathong S. 2008. Exploratory co-management interventions in Kuiburi National Park, Central Thailand, including human-elephant conflict mitigation. Intl J Environ Sustain Dev 7 (3): 293-310. DOI: 10.1504/ijesd.2008.021901.

Parracciani C, Gigante D, Bonini F, Grassi A, Morbidini L, Pauselli M, Valenti B, Lilli E, Antonielli F, Vizzari M. 2024. Leveraging Google Earth Engine for a more effective grassland management: A decision support application perspective. Sensors 24 (3): 834. DOI: 10.3390/s24030834.

Pastor J, Moen R, Cohen Y. 1997. Spatial heterogeneities, carrying capacity, and feedbacks in animal-landscape interactions. J Mammal 78 (4): 1040-1052. DOI: 10.2307/1383047.

Phumsathan S, Pongpattananurak N. 2021. Wildlife tourism management: Case study of the Kruger National Park, South Africa as a guideline for wildlife tourism management in Thailand. Thai J For 40 (2): 204-219. DOI: 10.14456/tjf.2021.27. [Thai]

Piipponen J, Jalava M, de Leeuw J, Rizayeva A, Godde C, Cramer G, Herrero M, Kummu M. 2022. Global trends in grassland carrying capacity and relative stocking density of livestock. Glob Change Biol 28 (12): 3902-3919. DOI: 10.1111/gcb.16174.

Poojary R, Raina R, Mondal AK. 2021. Effect of data-augmentation on fine-tuned CNN model performance. IAES Intl J Artif Intell 10 (1): 84-92. DOI: 10.11591/ijai.v10.i1.pp84-92.

Prayoon U, Suksavate W, Chaiyes A et al. 2024. Home range and habitat utilization of gaur (*Bos gaurus*) in transition zone between protected forest and human-dominated landscape, Eastern Thailand. Glob Ecol Conserv 50: e02811. DOI: 10.1016/j.gecco.2024.e02811.

Puspitasari RF, Aisyah, Khotimah U, Nugraha MR, Dzulfigar A, Marfi KP, Septianingrum D, Asy'ari R, Pramulya R, Zamani NP, Setyawan Y. 2024. Development of spatial platform based earth engine apps for mangrove carbon stock: Case study in Serang coastal zone, Banten Province. Celebes Agric 4 (2): 140-154. DOI: 10.52045/jca.v4i2.746.

QGIS.org. 2025. QGIS Geographic information system. Open Source Geospatial Foundation Project. http://qgis.org, accessed at 20 April 2025.

R Core Team. 2018. R: A language and environment for statistical computing. Foundation for Statistical Computing, Vienna, Austria. https://www.r-project.org/.

Rabinowitz A. 1989. The density and behavior of large cats in a dry tropical forest mosaic in Huai Kha Khaeng Wildlife Sanctuary, Thailand. Nat Hist Bull Siam Soc 37: 235-251.

Réjou-Méchain M, Muller-Landau HC, Detto M et al. 2014. Local spatial structure of forest biomass and its consequences for remote sensing of carbon stocks. Biogeosciences 11 (23): 6827-6840. DOI: 10.5194/bg-11-6827-2014.

Rischbeck P, Elsayed S, Mistele B, Barmeier G, Heil K, Schmidhalter U. 2016. Data fusion of spectral, thermal and canopy height parameters for improved yield prediction of drought stressed spring barley. Eur J Agron 78: 44-59. DOI: 10.1016/j.eja.2016.04.013.

Schirrmann M, Giebel A, Gleiniger F, Pflanz M, Lentschke J, Dammer K-H. 2016b. Monitoring agronomic parameters of winter wheat crops with low-cost UAV imagery. Remote Sens 8 (9): 706. DOI: 10.3390/rs8090706.

Schirrmann M, Hamdorf A, Garz A, Ustyuzhanin A, Dammer K-H. 2016a. Estimating wheat biomass by combining image clustering with crop height. Comput Electron Agric 121: 374-384. DOI: 10.1016/j.compag.2016.01.007.

Schreiber LV, Amorim JGA, Guimarães L, Matos DM, da Costa CM, Parraga A. 2022. Above-ground biomass wheat estimation: Deep learning with UAV-based RGB images. Appl Artif Intell 36 (1): 2055392. DOI: 10.1080/08839514.2022.2055392.

Schwarz C, Johncola A, Hammer M. 2020. Foraging ecology of semi-free-roaming Asian elephants in Northern Thailand. Gajah 52: 4-14. DOI: 10.5281/zenodo.4070864.

Shi X, Cao W, Raschka S. 2023. Deep neural networks for rank-consistent ordinal regression based on conditional probabilities. Pattern Anal Appl 26: 941-955. DOI: 10.1007/s10044-023-01181-9.

Shin H-C, Roth HR, Gao M, Lu L, Xu Z, Nogues I, Yao J, Mollura D, Summers RM. 2016. Deep convolutional neural networks for computer-aided detection: CNN architectures, dataset characteristics and transfer learning. IEEE Trans Med Imaging 35 (5): 1285-1298. DOI: 10.1109/tmi.2016.2528162.

Shorten C, Khoshgoftaar TM. 2019. A survey on image data augmentation for deep learning. J Big Data 6: 60. DOI: 10.1186/s40537-019-0197-0.

Singh M, Evans D, Friess DA, Tan BS, Nin CS. 2015. Mapping above-ground biomass in a tropical forest in Cambodia using canopy textures derived from Google Earth. Remote Sens 7 (5): 5057-5076. DOI: 10.3390/rs70505057.

Skerman PJ, Riveros F. 1990. Tropical Grasses. Food and Agriculture Organization of the United Nations, Rome.

Srikrachang M, Srikosamatara S. 2005. Elephant crop raiding problems and their solutions at Kui Buri National Park, Southwestern Thailand. Nat Hist Bull Siam Soc 53: 87-109.

Steinmetz R, Chutipong W, Seuaturien N, Chirngsaard E, Khaengkhetkarn M. 2010. Population recovery patterns of Southeast Asian ungulates after poaching. Biol Conserv 143 (1): 42-51. DOI: 10.1016/j.biocon.2009.08.023.

Steinmetz R, Seuanturien N, Srirattanaporn S, Poonnil B. 2011. Experimental Approaches Towards Tiger Recovery in Kuiburi National Park, Thailand. WWF Thailand and Department of National Parks, Wildlife, and Plant Conservation, Bangkok, Thailand.

Steinmetz R, Seuaturien N, Chutipong W, Poonnil B. 2009. The ecology and conservation of tigers and their prey in Kuiburi National Park, Thailand. WWF Thailand and Department of National Parks, Wildlife, and Plant Conservation, Bangkok, Thailand.

Steinmetz R, Seuaturien N, Srirattanaporn S, Poonnil B. 2012. Research and Conservation of Tigers and Their Prey in Kuiburi National Park. WWF, Thailand.

Steinmetz R, Srirattanaporn S, Mor-Tip J, Seuaturien N. 2014. Can community outreach alleviate poaching pressure and recover wildlife in South-East Asian protected areas? J Appl Ecol 51 (6): 1469-1478. DOI: 10.1111/1365-2664.12239.

Stockman G, Shapir LG. 2001. Computer Vision. Prentice Hall PTR, United States.

Stuth JW, Sheffield WJ. 1986. Determining Carrying Capacity for Combinations of Livestock, White-Tailed Deer, and Exotic Ungulates. Proceedings of the 1986 International Ranchers Roundup, Agricultural Extension Service, Texas.

Sukumar R. 1990. Ecology of the Asian Elephant in Southern India. II. Feeding habits and crop raiding patterns. J Trop Ecol 6 (1): 33-53. DOI: 10.1017/S0266467400004004.

Tanasarnpaiboon S. 2016. Gaur (*Bos gaurus*) Abundance, Distribution, and Habitat Use Patterns in Kuiburi National Park, Southwestern Thailand. [Dissertation]. University of Nebraska-Lincoln, Nebraska.

Tao Z, Yi L, Bao A, Xu W, Wang Z, Xiong S, Bing H. 2024. UAV or satellites? How to find the balance between efficiency and accuracy in above ground biomass estimation of artificial young coniferous forest? Intl J Appl Earth Obs Geoinf 134: 104173. DOI: 10.1016/j.jag.2024.104173.

Tekletsadik T, Tudsri S, Juntakool S, Prasanpanich S. 2004. Effect of dry season cutting management on subsequent forage yield and quality of ruzi (*Brachiaria ruziziensis*) and dwarf napier (*Pennisetum purpureum* L.) in Thailand. Agric Nat Resour 38 (4): 457-467.

Temchai T, Chamnankid C, Yoosomboon A. 2010. Habitat diversity and land use of Kuiburi National Park and Keangkrachan-Kuiburi National Park corridor. National Park and Protected Areas Innovation Center, Petchburi, Thailand.

Thai Meteorological Department. 2014. Climatological data of Prachaup Khirikhan Station. Thai Meteorological Department, Thailand.

Tian Y-C, Zhu Y, Cao W-X. 2005. Monitoring soluble sugar, total nitrogen and its ratio in wheat leaves with canopy spectral reflectance. Acta Agron Sin 31 (3): 355-360.

Tucker CJ. 1979. Red and photographic infrared linear combinations for monitoring vegetation. Remote Sens Environ 8 (2): 127-150. DOI: 10.1016/0034-4257(79)90013-0.

Umuhoza J, Jiapaer G, Yin H, Mind'je R, Gasirabo A, Nzabarinda V, Umwali ED. 2021. The analysis of grassland carrying capacity and its impact factors in typical mountain areas in Central Asia-A case of Kyrgyzstan and Tajikistan. Ecol Indic 131 (1): 108129. DOI: 10.1016/j.ecolind.2021.108129.

UNESCO. 2021. Kaeng Krachan Forest Complex. https://whc.unesco.org/en/list/1461.

Van Con T, Thang NT, Ha DTT, Khiem CC, Quy TH, Lam VT, Do TV, Sato T. 2013. Relationship between aboveground biomass and measures of structure and species diversity in tropical forests of Vietnam. For Ecol Manag 310: 213-218. DOI: 10.1016/j.foreco.2013.08.034.

Vapnik VN. 1995. The Nature of Statistical Learning Theory. Springer-Verlag, New York.

Vavra M. 2005. Livestock grazing and wildlife: Developing compatibilities. Rangel Ecol Manag 58 (2): 128-134. DOI: 10.2111/1551-5028(2005)58<128:LGAWDC>2.0.CO;2.

Vawda MI, Lottering R, Mutanga O, Peerbhay K, Sibanda M. 2024. Comparing the utility of Artificial Neural Networks (ANN) and Convolutional Neural Networks (CNN) on Sentinel-2 MSI to estimate dry season aboveground grass biomass. Sustainability 16 (3): 1051. DOI: 10.3390/su16031051.

Vieira EA, Galvão FCA, Barros AL. 2019. Influence of water limitation on the competitive interaction between two *Cerrado* species and the invasive grass *Brachiaria brizantha* cv. Piatã. Plant Physiol Biochem 135: 206-214. DOI: 10.1016/j.plaphy.2018.12.002.

Wang F-M, Huang J-F, Tang Y-L, Wang X-Z. 2007. New vegetation index and its application in estimating leaf area index of rice. Rice Sci 14 (3): 195-203. DOI: 10.1016/S1672-6308(07)60027-4.

Wang L, Zhou X, Zhu X, Dong Z, Guo W. 2016. Estimation of biomass in wheat using random forest regression algorithm and remote sensing data. Crop J 4 (3): 212-219. DOI: 10.1016/j.cj.2016.01.008.

Wickham H, Averick M, Bryan J et al. 2019. Welcome to the Tidyverse. J Open Source Softw 4 (43): 1686. DOI: 10.21105/joss.01686.

Wickham H. 2016. Ggplot2: Elegant Graphics for Data Analysis. Springer-Verlag, New York.

Wong CC, Sharudin MM, Rahim H. 1985. Shade tolerance potential of some tropical forages for integration with plantations. 1. Grasses Mardi Res Bull 13 (3): 225-247.

Zhu X, Chen X, Ma L, Liu W. 2024. UAV and satellite synergies for mapping grassland aboveground biomass in Hulunbuir Meadow Steppe. Plants 13 (7): 1006. DOI: 10.3390/plants13071006.

Zhu XX, Tuia D, Mou L, Xia G-S, Zhang L, Xu F, Fraundorfer F. 2017. Deep learning in remote sensing: A comprehensive review and list of resources. IEEE Geosci Remote Sens Mag 5 (4): 8-36. DOI: 10.1109/mgrs.2017.2762307.

Table S1. Augmentation parameters were applied in the digital image and UAV-based CNN model

Augmentation parameter	Setting
Rescale	multiply 1/255
Shear range	random with angle in [-30°, 30°]
Zoom range	random with zoom in [0.0,0.2]
Rotation range	random with angle in [-180°, 180°]
Width and height shift range	random with shift in [-0.2, 0.2]
Brightness range	random in [0.75, 1.00]
Fill mode	nearest
Flip	horizontal and vertical
Random contrast	factor value 0.3
Saturation	random with value in [0.5, 1.5]
Hue	random delta value 0.1
Random noise	random noise with zero mean and standard deviation in [0.0, 0.2]
Random shuffling of quadrants with randomly 90 degrees rotation	-
Random shadow	four corners of the polygon with adjusting the brightness factor are 0.7

Table S2. Multispectral image and vegetation indices on Sentinel-2 imagery are used to upscale biomass map

Type	Name	Abbreviation	Formula	Reference
Multispectral image	Aerosols	B1	-	
	Blue	B2	-	
	Green	B3	-	
	Red	B4	-	
	Red Edge 1	B5	-	
	Red Edge 2	B6	-	ESA (2014)
	Red Edge 3	B7	-	
	NIR	B8	-	
	Red Edge 4	B8A	-	
	Water vapor	B9	-	
	SWIR 1	B11	-	
	SWIR 2	B12	-	
Broadband vegetation index	Green normalized difference vegetation index	GNDVI	$\frac{(NIR - Green)}{(NIR + Green)}$	Gitelson et al. (1996)
	Green-blue normalized difference vegetation index	GBNDVI	$\frac{NIR - (Green + Blue)}{NIR + (Green + Blue)}$	Wang et al. (2007)
	Normalised difference vegetation index	NDVI	$\frac{(NIR - Red)}{(NIR + Red)}$	Tucker (1979)
	Soil adjusted vegetation index	SAVI	$\frac{(NIR - Red) \times (1 + L)}{(NIR + R + L)}$ Where L = 0.5	Huete (1988)
	Green soil-adjusted vegetation index	GSAVI	$1.5 \times \frac{NIR - Green}{NIR + Green + 0.5}$	Tian et al. (2005)
	Atmospherically resistance vegetation index	ARVI	$\frac{(NIR - Red)}{(NIR + Blue)}$	Kaufman and Tanré (1996)
	Chlorophyll green index	CGM	$\frac{NIR}{Green} - 1$	Gitelson and Merzlyak (1997)
	Simple ratio	SR	$\frac{NIR}{Red}$	Chen (1996)
	Modified simple ratio	MSR	$\frac{(NIR \div Red - 1)}{Sqrt(NIR \div Red) + 1}$	Chen (1996)
	Photosynthetic vigour ratio	PVR	$\frac{(Green - Blue)}{(Green + Blue)}$	Kobayashi et al. (2020)
	Transformed difference vegetation index	TDVI	$\sqrt{0.5 + \frac{(NIR - Red)}{(NIR + Red)}}$	Bannari et al. (2002)
	Normalized difference salinity index	NDSI	$\frac{(SWIR\,1 - SWIR\,2)}{(SWIR\,1 + SWIR\,2)}$	Dehni and Lounis (2012)
Red edge vegetation index	Anthocyanin reflectance index	ARI	$\frac{1}{Green} - \frac{1}{RE1}$	Gitelson et al. (2009)
	Normalised difference red edge2	NDRE2	$\frac{(RE2 - Red)}{(RE2 + Red)}$	Gitelson and Merzlyak (1994)
	Normalised difference red edge3	NDRE3	$\frac{(RE3 - Red)}{(RE3 + Red)}$	Gitelson and Merzlyak (1994)
	Normalised difference red edge8a	NDRE8a	$\frac{(RE8a - Red)}{(RE8a + Red)}$	Gitelson and Merzlyak (1994)
	Red edge chlorophyll index	RECI	$\frac{RE3}{RE1} - 1$	Gitelson et al. (2003)
	Chlorophyll absorption ratio index	CARI	$\frac{RE1 \times \sqrt{(a \times Red + Red + b)^2}}{Red} \times (a^2 + 1)^{0.5}$ Where a = (RE1 - Green)/150, b = Green×550×a	Kim et al. (1994)